Prediction of mechanical properties of carbon nanotubecarbon fiber reinforced hybrid composites using multi-scale finite element modelling

# Prediction of Mechanical Properties of Carbon Nanotube–Carbon Fiber Reinforced Hybrid Composites Using Multi-Scale Finite Element Modelling

**Reza Malekimoghadam**[*], **Ugo Icardi****

[1] Department of Mechanical and Aerospace Engineering, Politecnico di Torino, Torino, Italy

## Abstract

The mechanical properties of unidirectional carbon nanotube (CNT)–carbon fiber (CF) reinforced hybrid composites are scrutinized. Due to lack of comprehensive model, a 3D multi-scale model considering debonding damage is developed, covering from nano- to macro-scale. Considering three different configurations of grown CNT's on the fiber surface, the interfacial behavior is investigated. The results reveal that : (I) an extraordinary influence of CNT's on the fiber-matrix interfacial properties, particularly in the composites containing axially and randomly oriented CNT's, (II) considering two hybrid systems, composites with CNT's–coated fibers demonstrate outstanding improvements in the interfacial behaviors than those with CNT's in matrix, (III) the pronounced effect of non-bonded interphase region on the interfacial properties, while no influence on the Young's moduli is observed, and (IV) the presence of CNT's augments the transverse Young's modulus, however, it exhibits negligible effect on the longitudinal direction. The outcomes are consistent with experimental data and can be utilized in designing of CNT–CF multi-scale composites.

**Keywords:** Carbon Nanotube–Carbon Fiber Hybrid Composites; A: Nano-structures; B: Interface/interphase; B: Debonding; C: Finite element analysis (FEA)

[*] Corresponding Author. *Email Address:* reza.malekimoghadam@polito.it, reza.malekimoghadam@gmail.com
** Corresponding Author. *Email Address:* ugo.icardi@polito.it

## 1. Introduction

As a fundamental issue, fiber-matrix interfacial properties extraordinarily influence on the mechanical behavior and load transferring phenomenon of composite structures [1–6]. Multifarious experimental, computational and analytical investigations have been carried out in order to characterize and ameliorate the interfacial and interlaminar properties of composite structures [7–13]. Thus, improvement of fiber-matrix interfacial properties plays a momentous role which augments the overall mechanical behaviors, however, with poor interfacial strength, debonding occurs, resulting in a weaker composite structure [14,15]. On the other hand, breakthrough of carbon nanotubes (CNTs) and nano-particles have flourished a novel research sphere among scientists because of their unique properties [16–23]. It has been demonstrated that dispersion of a few portion of carbon nanotubes in a matrix, increase remarkably the mechanical properties of composite materials [24–27]. Having implemented various experimental tests, noticeable growth in the mechanical properties of polymers have been reported in the literatures by incorporating 1–5% weight fractions of CNT's[28,29]. Owing to the exceptional characteristics of carbon nanotubes, by incorporating CNT's, multi-scale hybrid composites are being developed due to their outstanding behaviors in obviating cardinal drawbacks of conventional composites regarding interfacial and interlaminar properties, by altering the fiber-matrix interface region [30]. Depending on the dispersion of CNT's in the hybrid composites, it can be categorized into two types of systems encompassing 'mixed CNT/matrix system' and 'hybrid fiber system', while in the former the CNT's are mixed with resin, whereas in latter the forest of carbon nanotubes are grown on the surface of core fibers, so-called fuzzy-fiber reinforced composites (FFRC) [31,32]. Introducing small portion of carbon nanotubes on the surface of carbon fiber, significant enhancement of interfacial shear strength (IFSS) and interlaminar shear strength (ILSS) were attained by 89.4% and 58.6%, respectively, by Yao et. al [33]. In addition to the significant influence of FF's on the interfacial properties between fiber and matrix, a basic drawback of unidirectional fiber reinforced composites ascribed to the low mechanical properties in the transverse direction to the fiber can be overcome by presence fuzzy fibers [34]. From experimental investigation point of view, some researches have been accomplished in order to study the mechanical, thermal and electrical properties and health monitoring applications of fuzzy fiber reinforced hybrid composites [35–37]. Growing the graphene oxide and carbon nanotubes on the carbon fiber surface, the interfacial properties have experimentally been investigated in the recent

literatures [38,39]. The outcomes divulged that all the foregoing nano-reinforcements, noticeably improve the interfacial and interlaminar properties of composites with only small portion of nano-materials. Conducting a survey on the influence of the growth temperature and time of CNT on the fiber- matrix interfacial shear strength (IFSS), by Aziz et al. [40], the temperature of 700º with 30 minutes reaction time has exhibited the noticeable IFSS. Garcia and his co-worker [41,42]conducted a survey on the morphology control of aligned CNT's on the fibers and improving the interlaminar strength of prepreg unidirectional carbon tape composites by exploiting the bridging effect of aligned CNT's. From multi-scale modeling point of view, some analytical investigations have been implemented considering some assumptions, however, due to novelty and complexity of such nano-engineered multi-scale materials, there still exist many aspects which should be clarified and characterized unambiguously [43–45]. A general micromechanics method was developed by Chatzigeorgiou et al.[46], in order to attain the elastic moduli of hybrid composites consisting of carbon fiber coated with radially aligned CNT's. The results disclosed enhancement of elastic moduli by increasing the volume fraction of carbon fiber and CNT's. Investigating the fatigue behavior of CF/ CNT hybrid composite, Dai and Mishnaevsky Jr. [47] carried out a finite element modeling in which superior fatigue performance was observed than those without CNT's reinforcements. Finite element analysis and experimental investigation were conducted by Kulkarni et. al [48] in order to acquire the elastic moduli of CNT/ CF hybrid composites. Considering CNT/CF as a homogeneous solid model with larger diameter, it was determined that multiscale modeling can be effectively used to study nanoreinforced laminated composites. Kundalwal and collaborators [49–54] studied the thermoelastic and mechanical properties of hybrid composites considering straight and waviness CNT's invoking micromechanics modeling. The results demonstrated remarkable enhancement in transverse young modulus and coefficients of thermal expansion of the CNT/ CF composite. Deeming homogeneous cylindrical inclusion as effective fuzzy fiber tow, Ren et al. [55] characterized the piezoresistive response of fuzzy fiber reinforced composite by computational modeling considering radially aligned CNT and interphase region as continuum mediums. In accordance with the aforementioned literatures, majority of them were dedicated to the elastic moduli of hybrid composites. Furthermore, a detailed 3D multi-phase model which is capable of capturing all length-scale parameters and considering CNT's orientations and debonding is lacking. Hence, in order to scrutinize the mechanical properties of CF–CNT hybrid composite, particularly interfacial

properties, the present work proposes a 3D multiscale finite element (FE) model of carbon fiber-carbon nanotube reinforced hybrid composites, taking into account all the parameters covering from nano- to macro-scale and considering debonding damage between CNT's and surrounding matrix. Moreover, current research demonstrates the remarkable effect of grown CNT's on the interfacial shear and radial stresses considering three different orientations of CNT's, which is significant from fiber-matrix interfacial adhesion point of view. Meanwhile, the influence of two different hybrid systems including 'hybrid fiber system' and 'mixed CNT/matrix system' on the interfacial properties are assessed. The nonlinear finite element analysis is also validated by user-defined FE code prepared in the current work and published experimental data on the elastic moduli.

## 2. Framework of Computational Multi-Scale Modeling

There are different techniques for the deposition of CNT's on the surface of carbon fiber consisting of Chemical Vapor Deposition (CVD), electrophoresis, etc. which possess their advantageous and limitations [56]. Although by systematically varying the catalyst concentration, catalyst pre-treatment time, and sample position within the tube furnace, the key factors governing CNT morphology could be likely achievable [57], CNT's are predominantly grown in radial and randomly orientations on the fiber surface [58].The presence of CNT's forest on the surface of the fiber is depicted in Fig.1, in which the left and right pictures are relevant to predominantly radially and randomly oriented CNT's, respectively. In order to scrutinize the influence of CNT morphology on the mechanical properties of hybrid composite, therefore, CNT's with radially, axially and randomly orientations are taking into account in the present work.

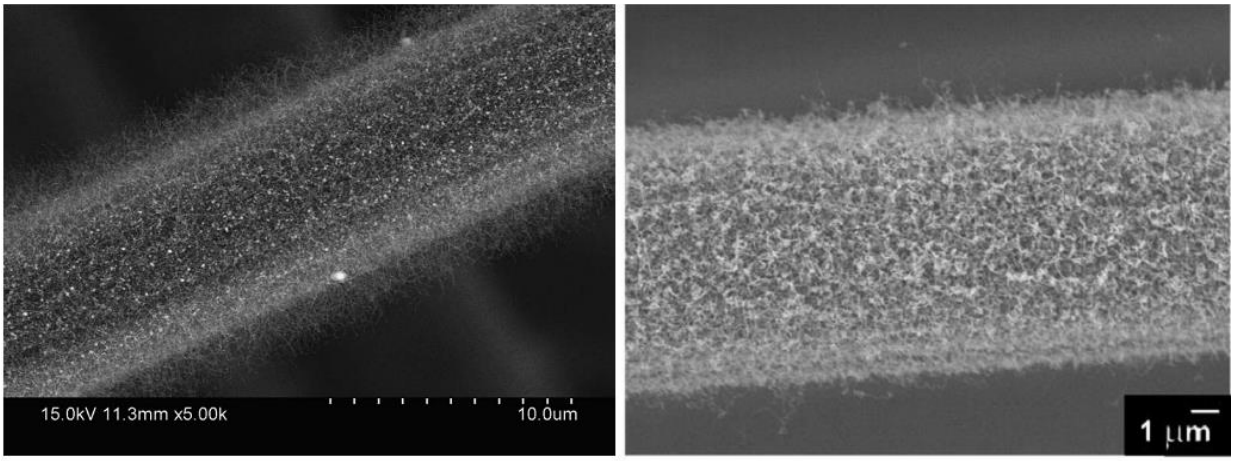


**Fig. 1:** A single fuzzy fiber with predominantly radially oriented CNT's (left) [36] and randomly oriented CNT's (right) on the surface of the carbon fiber [31]

Due to above-mentioned statements, irrefutably, the multiscale architecture of the fuzzy fiber reinforced composites (FFRC) can be quite complex. Therefore, a concurrent 3D multiscale finite element model has been proposed in the present work considering all length scale from nano to macro, in which the fine scale is directly embedded in the coarse scale simultaneously, excluding homogenized or effective/ equivalent material which the latter is usually employed by hierarchical approach. The proposed model is capable of capturing of the characteristics at each scale and taking into account the crucial features of the model comprising the CNT volume fraction, CNT's orientations, debonding between CNT's and matrix and fiber volume fraction in the hybrid composite. It is noteworthy to mention that the debonding damage between CNT's and surrounding matrix is simulated via cohesive zone model (CZM) considering mixed mode traction-separation law, while no fracture phenomenon or crack opening has been taken into account. Otherwise, in case of considering fracture in multi-scale modeling, the transfer of length scales and issues related to size effects will play a critical role [59,60].

Hence, in order to furnish an efficacious insight towards the design of FFRC with measurable and adjustable parameters, these features are profoundly investigated. The multiscale framework of fuzzy fiber hybrid composite is delineated in Fig.2. It is noteworthy to mention that a user-defined linear finite element formulation is also constructed in order to certify the elastic modulus obtained via concurrent multi-scale modeling which is elaborate in section.3.

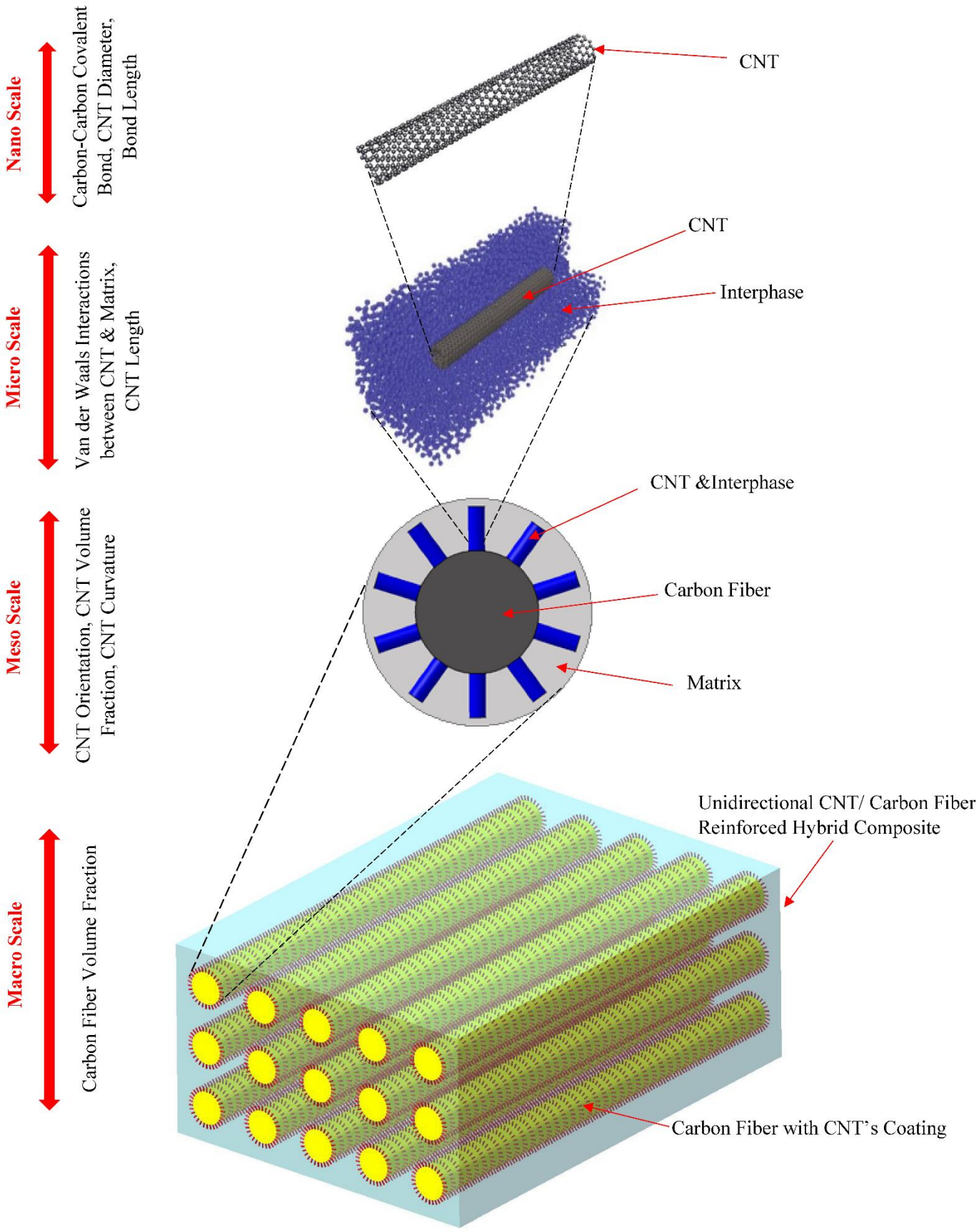




**Fig. 2:** The multi-scale modeling framework of hybrid composite and effective parameters at each scale

## 2.1. Nano-Scale Modelling

At nano-scale, CNT's act as nano-reinforcement agent in the hybrid composite. The theoretical efforts in modeling CNT behavior can be classified in three categories as atomistic modeling, continuum modeling and nano-scale continuum modeling [61]. Various approaches in the modeling of carbon nanotube were rigorously reviewed and analyzed by Rafiee and Malekimoghadam [16] concentrating on mechanical, buckling, vibrational and thermal properties. Developing a finite element model of the CNT lattice structure by Li and Chou [62], each Carbon–Carbon bond of the CNT nanostructure is replaced with equivalent beam element in which the geometrical and mechanical properties of the beam element are obtained correlating the interatomic potential energies of molecular space to the strain energies of structural mechanics. Different researchers applied continuum shell models to study the CNT properties [63,64] which the outcomes imply the similarities between MD simulation of CNTs and macroscopic shell model. Bagchi and Nomura [65] were developed a model predicting the effective thermal conductivity of multi-walled nanotube polymer composite considering an equivalent shell model as CNT structure. Choi et al. [66] considered a transversely isotropic hollow cylinder solid model for finite element modeling of vibration behavior of multi-walled carbon nanotube. Consequently, in the current research the multi-walled carbon nanotube is simulated as a transversely isotropic shell structure with thickness of 0.34nm [61,67]. The required mechanical properties of carbon nanotube for finite element modeling are summarized in the Table.1 [68,69].

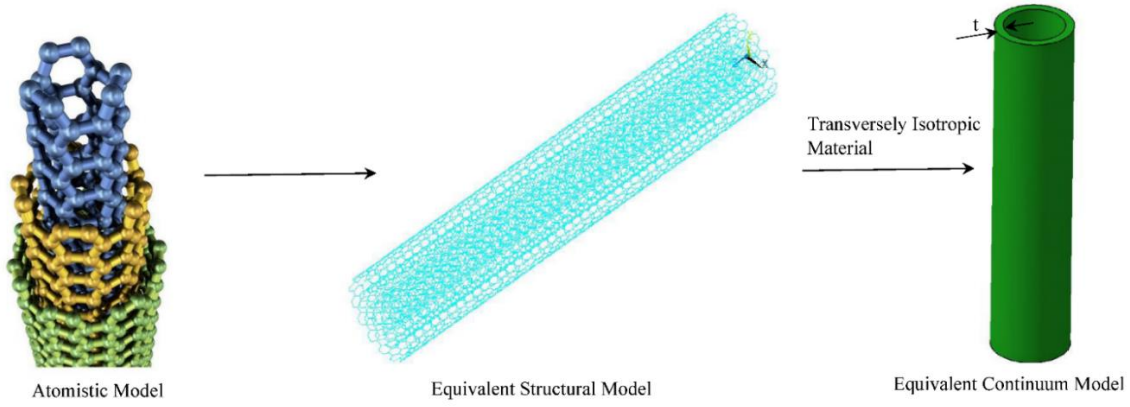


**Fig. 3:** Equivalence molecular, finite element and continuum models

Table 1: Mechanical properties of Carbon Nanotube

| Material | $E_z$ [TPa] | $E_x$, $E_y$ [GPa] | $G_{xz}$, $G_{yz}$ [GPa] | $G_{xy}$ [GPa] | $\upsilon_{xz}$, $\upsilon_{yz}$ | $\upsilon_{xy}$ |
|---|---|---|---|---|---|---|
| CNT | 1.3 | 40 | 440 | 13 | 0.19 | 0.469 |

### 2.2. Interface Region between Carbon Nanotube and Surrounding Matrix

From atomistic point of view, the governing interactions between CNT and surrounding polymer are weakly non-bonded vdW interactions in absence of chemical functionalization, in which no covalent bonding is produced [70]. From structural point of view, two different approaches can be found in literatures for simulating interphase either as a continuum or as a discrete region exerting continuum hollow cylinder and truss/ nonlinear beam elements, respectively [71,72]. The vdW interactions are mostly modeled using Lennard–Jones (L–J) ‘‘6–12” potential [73]. Utilizing nonlinear springs representing interphase region based on L-J potential, a multi-scale model of carbon nanotube reinforced composite was proposed by Rafiee and Malekimoghadam [74]. Due to inherently nonlinear behavior of vdW interactions, it could be simulated either by non-linear springs or cohesive zone model which the latter method has been adopted for this research. Based on the Lennard–Jones ‘‘6–12”, the vdW force in term of interatomic distance is presented by following equation [73].

$$V_{LJ}(r) = 4\varepsilon\left[\left(\frac{\sigma^{12}}{r}\right) - \left(\frac{\sigma^{6}}{r}\right)\right] \quad (1)$$

where ε and σ are the Lennard–Jones parameters as 0.4492 kJ/mol and 0.3825 nm, respectively [73]. It should be noted the vdW interaction can be neglected when the inter-atomic distance is equal or greater than 0.85 nm [71]. Based on the L–J potential for the van der Waals interaction, the following cohesive law for CNT/polymer interfaces has been established as Eq. (2) [75].

$$\sigma^{int} = 3.07\sigma_{max}\left[\left(1 + 0.682\frac{\sigma_{max}}{\varphi_{total}}[u]\right)^{-4} - \left(1 + 0.682\frac{\sigma_{max}}{\varphi_{ottal}}[u]\right)^{-10}\right] \quad (2)$$

where $\sigma^{int}$ and [u] are the normal cohesive stress and opening displacement at the CNT/polymer interface, respectively. Furthermore, the cohesive strength ($\sigma_{max}$) and total cohesive energy( $\varphi_{total}$) are denoted by the below equations based on the parameters σ and ε in the L–J potential.

$$\sigma_{max} = \frac{6\pi}{5}\rho_p\rho_c\varepsilon\sigma^2 \quad (3)$$

$$\varphi_{total} = \frac{4\pi}{9}\sqrt{\frac{5}{2}}\rho_p\rho_c\ \ \varepsilon\sigma^3 \quad (4)$$

Where $\rho_c$ and $\rho_p$ are the CNT area density and the polymer volume density which equal $3.82 \times 10^{19}$ $m^{-2}$ and $3.1 \times 10^{28}$ $m^{-3}$, respectively [76]. It is worth mentioning that Eq. (3) represents a rather high cohesive strength, however, Eq. (4) exhibits a very low cohesive energy $\varphi_{total}$ = 0.107 Jm-2, which is in correlation with the poor bonding between CNTs and encircling polymer. The normal cohesive stress versus the interface opening displacement is depicted in Fig.4 [76] in which the cohesive ascends rapidly at the maximum of 475 MPa at small opening displacement of 0.0542 nm.

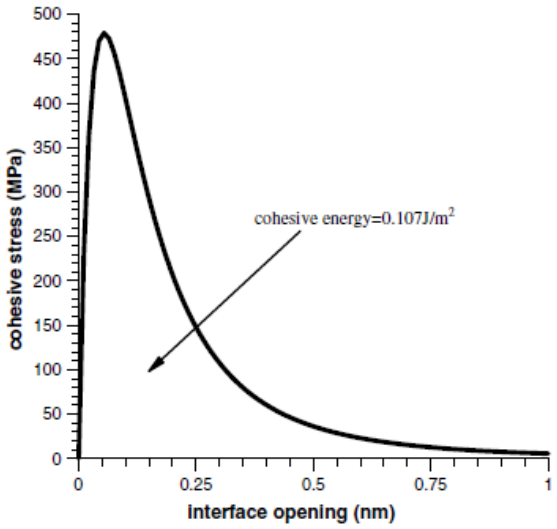


**Fig. 4:** The cohesive law for a carbon nanotube and polymer matrix established from the van der Waals interactions at the nanotube/matrix interface.

Some literatures [21,77] have calculated the interfacial shear strength of the CNT's pull out from the matrix using MD simulation and experimental investigations. Different interfacial constitutive relations for various shapes of traction-separation curves, such as exponential, bilinear and polynomial have been proposed by the researchers [78]. In the current research, the bilinear cohesive zone material (CZM) is introduced as non-bonded Van der Waals interactions at the interphase region between CNT and surrounding matrix, employing the zero thickness INTER204

3D element. This element is defined by 16 nodes having three degrees of freedom at each node in the x, y, z directions as shown in Fig. 5 [79]. Likewise, it is capable of simulating an interface between two surfaces and the subsequent debonding damage process, where the separation is represented by an increasing displacement between initially coincident nodes, within the interface element itself. The CZM model consists of a constitutive relation between the traction "T" acting on the interface and the corresponding interfacial separation "δ" (displacement jump across the interface). Thus, the mixed mode bilinear cohesive law is exploited to simulate non-bonded interphase region between CNT's and matrix, in which the separation of material interfaces depends on both the normal and tangential components of displacement jumps which are displayed in Fig. 5. Given that the difference in the normal and tangential jumps contributions to the separation of material interfaces, a non-dimensional effective displacement jump λ for mixed-mode fracture is defined.

The normal and tangential components of cohesive tractions and corresponding relations in mixed-mode type are expressed as [79,80]:

$$T_n = K_n \delta_n (1-D_m) \tag{5}$$

$$T_t = K_t \delta_t (1-D_m) \tag{6}$$

$$\lambda = \sqrt{(\frac{\delta_n}{\delta_n^c})^2 + \beta^2 \left(\frac{\delta_t}{\delta_n^c}\right)^2} \tag{7}$$

$T_n$, $T_t$, $\delta_n$, $\delta_t$, $D_m$ describe normal traction, tangential traction, normal separation, tangential separation and damage parameter, respectively.

The β is the non-dimensional parameters which assigns different weights to tangential and normal displacement jumps. The damage parameter associated with mixed-mode bilinear cohesive law is illustrated as:

$$D_m = \begin{cases} 0 & \lambda_{max} = \lambda_\alpha \\ Min\ (1, dm) & \lambda_{max} > \lambda_\alpha \end{cases} \tag{8}$$

Where:

$$\lambda_{cr} = \frac{\delta_n^*}{\delta_n^c} = \beta\frac{\delta_t^*}{\delta_t^c} \tag{9}$$

$$d_m = \eta\left[\frac{\lambda max - \lambda cr}{\lambda max}\right] \tag{10}$$

$$\eta = \frac{\delta_n^c}{\delta_n^c - \delta_n^*} = \frac{\delta_t^c}{\delta_t^c - \delta_t^*} \tag{11}$$

Where $\delta_n^c$ / $\delta_t^c$ and $\delta n^*$/ $\delta_t^*$, indicate normal/tangential displacement jump at the completion of debonding and normal/tangential displacement jump at maximum normal cohesive traction, respectively.

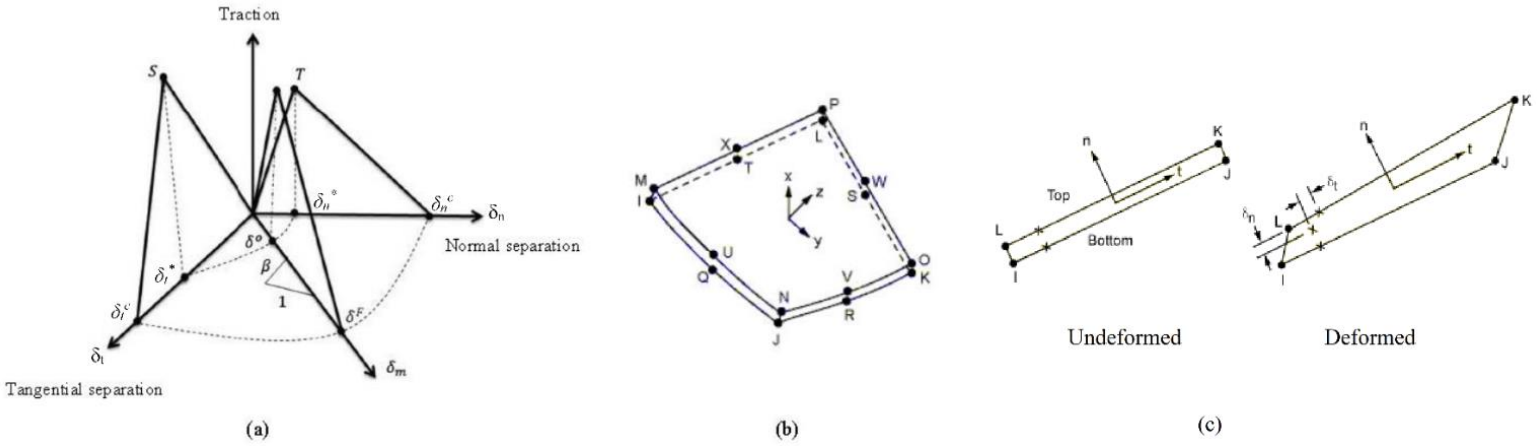


**Fig. 5**. Cohesive zone material (a) Mixed-mode traction-separation behavior (b) INTER204 3D element geometry (c) Defining tangential and normal directions through the element

Based on foregoing investigations, the maximum normal and shear interfacial strengths can be acquired for cohesive modeling [76,77]. There are six basic parameters to define the bilinear mixed-mode cohesive law in ANSYS which are depicted in Table.2, provided by the Van der Waals interactions. Recalling the aforementioned parameters, the α and β can be attained accordingly:

$$\alpha = \frac{\delta_n^*}{\delta_n^c} = \beta\frac{\delta_t^*}{\delta_t^c} \tag{12}$$

$$\beta = \frac{\delta_n^* \times \delta_t^c}{\delta_n^c \times \delta_t^*} \tag{13}$$

Table 2: The input values of Cohesive Model for finite element modeling

| $T^{n}_{max}$[MPa] | $\delta^{c}_{n}$[nm] | $T^{t}_{max}$[MPa] | $\delta^{c}_{t}$[nm] | α | β |
|---|---|---|---|---|---|
| 479 | 1 | 75 | 1.2 | 0.0542 | 0.0766 |

### 2.3. Finite Element Modeling of CNT/ CF Hybrid Composite

The dense of carbon nanotubes, practically, can be grown in different direction such as radially and randomly oriented [57], on the core fiber which will reflect different improvement in the properties of fuzzy fiber reinforced composites. Therefore, investigating the properties of FFRC with different CNT's orientation is a great of importance in such materials as well as accounting debonding damage between CNT and matrix. Hence three different cases of FFRC is considered in this research, in which the carbon nanotubes are radially aligned with respect to the fiber axis, axially aligned with respect to the fiber axis and randomly oriented, which are portrayed in Fig.6.

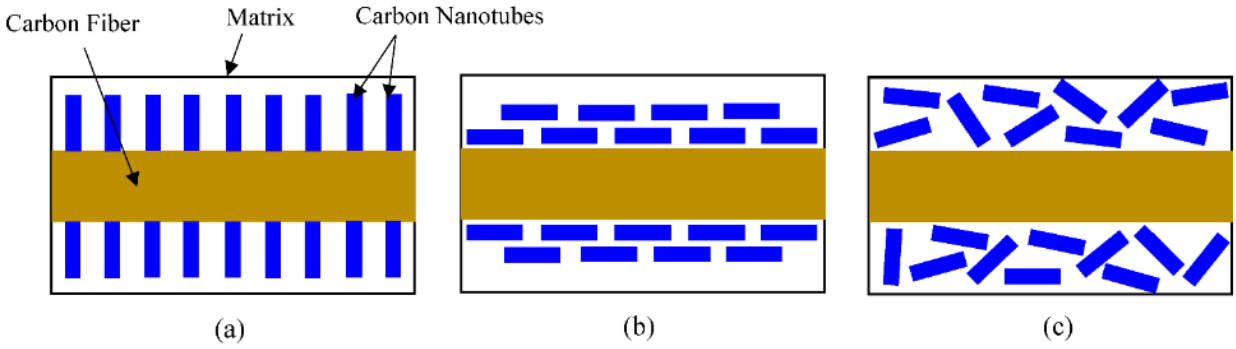


**Fig. 6:** Schematic illustration of carbon nanotube configuration around core fiber (a) radially aligned CNT's (b) axially aligned CNT's (c) randomly distributed CNT's

It should be mentioned that carbon fiber is simulated as transversely isotropic material and surrounding matrix is consider as a homogeneous isotropic material. The properties of carbon fiber are inserted in Table.3 [81,82]. Considering the volume fraction of carbon fiber, the dimensions of surrounding matrix has been obtained and both core fiber and matrix have been simulated using solid element (SOLID 186) [79]. The element possesses three degrees of freedom per each node including translational in x, y and z directions which can tolerate irregular shapes without loss of accuracy due to usage of intermediate nodes on each edge of the element and therefor higher order shape function.

Table 3: Elastic Properties of Carbon Fiber

| Material | $E_z$ [GPa] | $E_x$, $E_y$ [GPa] | $G_{xz}$, $G_{yz}$ [GPa] | $G_{xy}$ [GPa] | $\upsilon_{xz}$ | $\upsilon_{xy}$ |
|---|---|---|---|---|---|---|
| Carbon Fiber | 230 | 28.7 | 25 | 7 | 0.3 | 0.42 |

It worth mentioning that the CNT's orientation is controlled by defining local coordinate system in which the CNT longitudinal axis is parallel with the Z direction of local coordinate system whereas the longitudinal direction of carbon fiber is located in the Z direction of global coordinate system. Given that the CNT's are transversely isotropic materials with different orientations, therefore, the material properties of CNT's are defined on the local coordinate system. A schematic illustration of fuzzy fiber reinforced composite with corresponding global and local coordinate systems are delineated in Fig.7. Thus, hundreds of hollow cylinders should be constructed via the finite element model taking into account CNT's volume fraction and orientations. Recalling from previous section, carbon nanotubes are modeled as transversely isotropic material, consequently, a macro code has been written via ANSYS Parametric Design Language (APDL) in which a specific local nodal coordinate system and a specific local element coordinate system are defined for each CNT with respect to the CNT orientation. Having defined the local nodal and local element coordinate systems, the mechanical properties of each CNT are then introduced in the finite element model consecutively.

The dense of the CNT's which should be constructed in the finite element model leads to the massive computational analysis specially in the higher volume fraction. Hence, for 'radially aligned' and 'axially aligned' types of CNT's orientations, 'Cyclic Symmetric Analysis' technique has been adopted due to inherently axisymmetric circumstance of the foregoing CNT's configurations [79].

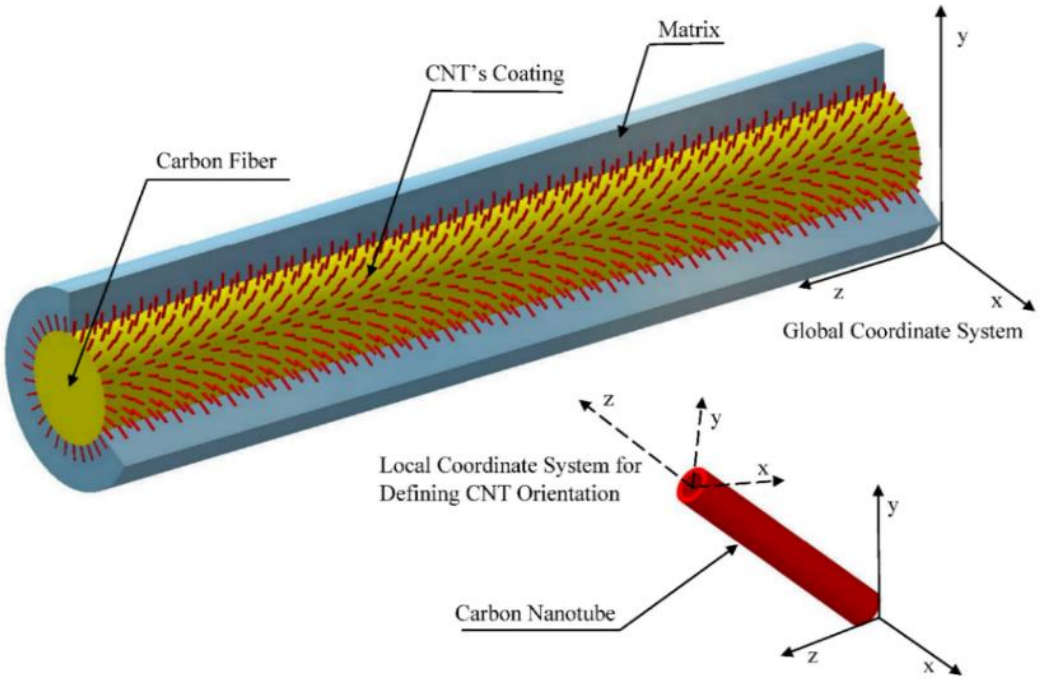


**Fig. 7:** Schematic illustration of fuzzy fiber reinforced composite RVE with corresponding global and local coordinate systems

Cyclic symmetry modeling is an analysis tool utilized to simulate structures having a repetitive geometric pattern in 360 degrees around an axis of symmetry. In order to execute the cyclic symmetry analysis, a single sector should be simulated, called the 'basic sector' which represents one part of a pattern. The angle α spanned by the basic sector should be such that $N\alpha = 360$, where $N$ is an integer. It should be indicated the complete model will be achieved by repeating $N$ times of basic sector in cylindrical coordinate space. Since the hybrid composite with randomly oriented CNT's is not an axisymmetric model, therefore 'Cyclic Symmetric Analysis' is not capable of simulating of such RVE model. Ergo, exerting random normal distribution, a macro code has been developed in order to generate the positions and orientations of carbon nanotubes. It should be indicated that in order to model the random oriented CNT's reinforced hybrid composite, the condition of the minimum surface to surface distance between two adjacent CNTs which is the equilibrium van der Waals distance as 0.34 nm, should be met. Nonetheless, by altering the momentous parameters of growth process, various morphologies of CNT organization on the fiber surface will be observed comprising entangled growth, locally-group growth and Mohawk morphology [57]. The finite element models of CF–CNT hybrid composite with three configurations of CNT's around carbon fiber are shown in Fig.8.

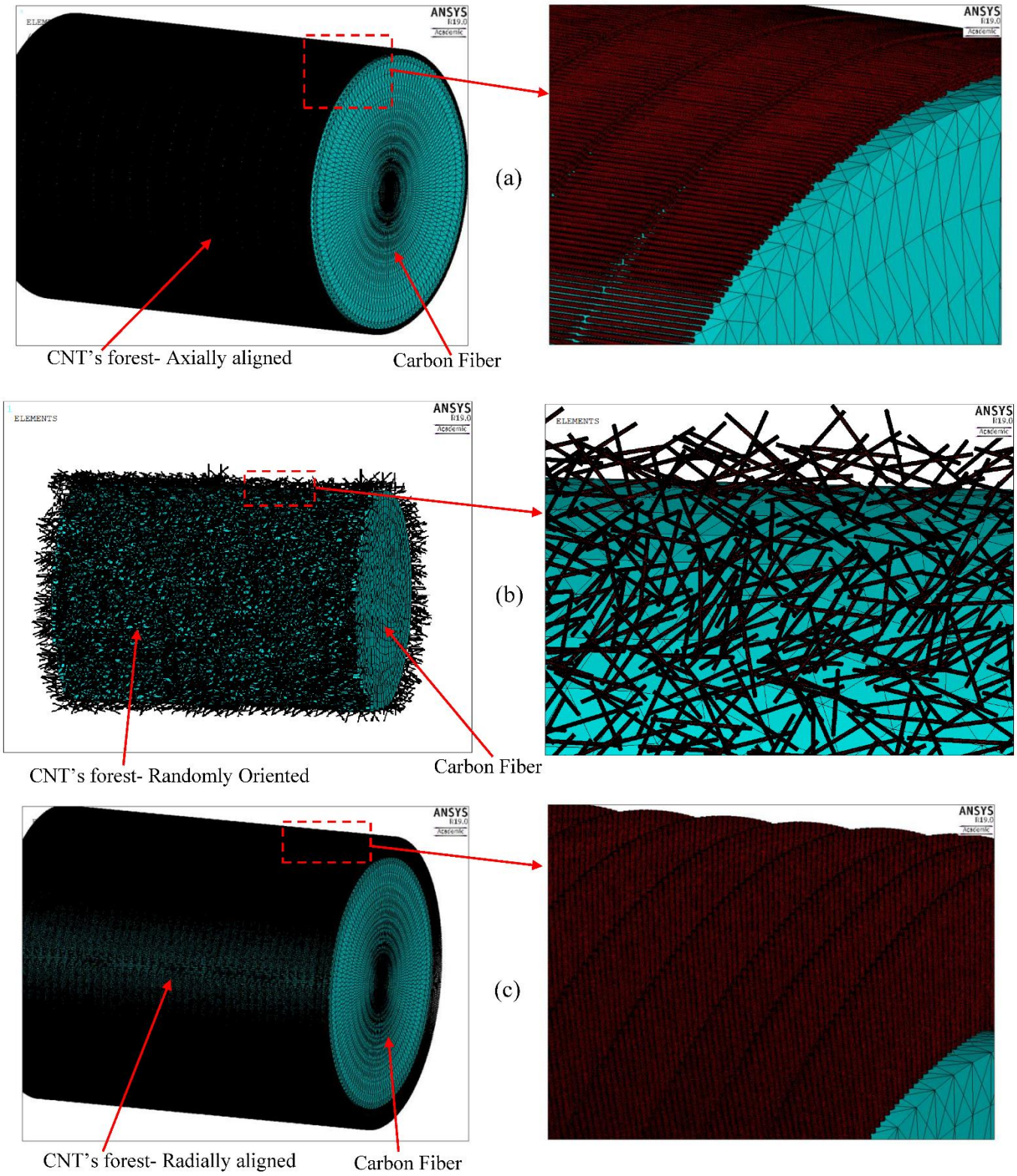


**Fig. 8:** Finite element model of CF–CNT hybrid composite (a) with axially aligned CNT's, (b) with randomly oriented CNT's (c) with radially aligned CNT's

## 3. User-Defined Finite Element Formulation

### *3.1. RVE model construction*

In order to obtain the elastic moduli of the hybrid composite and comparing with nonlinear concurrent multi-scale modeling, a user-defined finite element code is developed via MATLAB. Thus, a RVE is established through three concentric cylinders consisting of core fiber, micro-interphase region and surrounding matrix in which the micro-interphase contains matrix and randomly oriented CNT's. It should be mentioned that at this section, the carbon nanotube and interphase region are constructed as a nano–fiber utilizing equivalent continuum modeling technique [25,74]. Consequently, Mori-Tanaka model [83] is employed in order to determine the effective elastic properties of micro-interphase region which is required as input to user-defined finite element formulation. It should be notified that the details of Mori-Tanaka schemes for different types of inclusions and multi-phase systems have thoroughly been explicated in some literatures [84,85]. Exerting the Mori-Tanaka method and taking into account the average over orientations of nano-fibers, the effective stiffness tensor of micro-interphase region is defined accordingly [86]:

$$\mathrm{C}=\mathrm{C}_1+\sum_{\mathrm{r}=2}^{N} v_r \left\{\left(\mathrm{C}_r-\mathrm{C}_1\right):\mathrm{T}_r\right\}:\left[\sum_{\mathrm{r}=1}^{N} v_r \left\{\mathrm{T}_r\right\}\right]^{-1} \tag{14}$$

where C is the stiffness tensor of the composite which here is considered as micro-interphase region, $C_1$ and $C_r$ indicate the stiffness tensors of the matrix and the $r_{th}$ phase, respectively, and N denotes the number of the types of the reinforcements which in the present work is CNT. The volume fraction of the $r_{th}$ phase, is indicated by $v_r$. The Curly brackets {*} represent an average over all possible orientations. The tensor $T_r$ is designated as:

$$\mathrm{T}_r=\left[\mathrm{I}+\mathrm{S}_r:\mathrm{C}_1^{-1}:\left(\mathrm{C}_r-\mathrm{C}_1\right)\right]^{-1} \tag{15}$$

where I is the fourth-order symmetric unit tensor and $S_r$ is the Eshelby tensor. Accounting micro-interphase region as a two-phase composite including nano-fibers and matrix, Eq (14) is then rewritten:

$$C = C_1 + v_2\left\{(C_2 - C_1) : T_r\right\} : \left[v_1 I + v_2\left\{T_2\right\}\right]^{-1} \quad (16)$$

Where $v_1$ and $v_2$ indicate the volume fractions of matrix and CNT, respectively. The detailed expressions of $S_r$ for various shapes of inhomogeneities has entirely been illustrated by Mura [87]. Pursuant to the present work, the elements of Eshelby tensor are represented in Appendix A, considering cylindrical inclusion. Considering the randomly orientated CNTs in the micro-interphase region, the acquired properties signify the isotropic behavior of this region. Thus, in order to establish the user-defined FE formulation, the carbon fiber is modeled as transversely isotropic materials while the matrix and micro-interphase region are simulated as two discrete homogeneous isotropic mediums.

### 3.2. *Element formulation*

Employing a mixed eight-nodes element with six degree of freedom comprising three displacements and the three interlaminar stresses, the linear finite element analysis is conducted in order to obtain the elastic modulus of hybrid composites and making a comparison with nonlinear concurrent FEM which developed in the previous section. It is worthwhile to indicate that the statements of mixed formulation FE was comprehensively elaborated by Icardi and Atzori [88], therefore, hereafter the procedure will be summarized in this section.

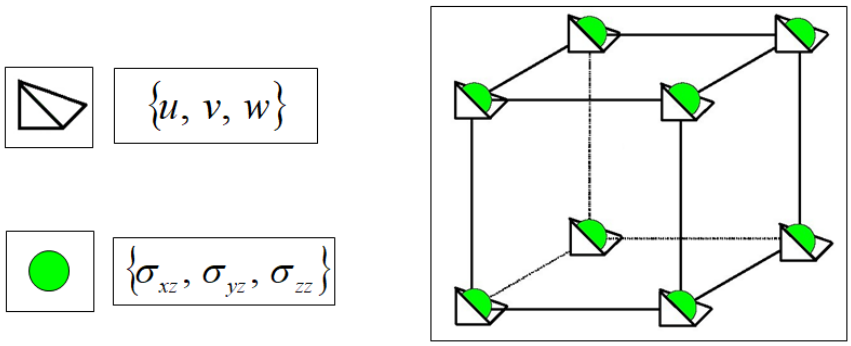


**Fig. 9:** 8-nodes brick elements with relevant degrees of freedom

Enthusiastically, Hellinger–Reissner (HR) functional $\Pi_{HR}$ [89] is introduced, by which the displacements and stresses are allowed to be varied separately that establishes the master fields.

The slave fields are the strains $e^{\sigma}{}_{ij}$ and $e^{u}{}_{ij}$ by the stress–strain and strain–displacement relations, respectively:

$$e^{u}{}_{ij} = \frac{1}{2}(u_{i,j} + u_{j,i}); \quad e_{ij}{}^{\sigma} = C_{ijkl}\,\sigma_{kl} \tag{17}$$

The functional $\Pi_{HR}$ is expressed as:

$$\Pi_{HR}(u_i, \sigma_{ij}) = \int_V \left( \sigma_{ij} e_{ij}{}^{u} - \frac{1}{2}\sigma_{ij} C_{ijkl} \sigma_{kl} - b_i u_i \right) dV - \int_{S_t} \hat{t}_i u_i \, dS \tag{18}$$

where $b_i$ and $t_i$ represent the volume forces and the surface tractions, respectively.

From stability standpoint, the finite elements based on mixed formulations is governed by rather complex mathematical relations, as discussed by Babuska [90]. Notwithstanding relaxation of continuity requirements, certain choices of the individual shape functions could not lead to meaningful results in mixed formulations which is a consequence of the so-called Babuska–Brezzi [90] criterion for stability. In order to eschew occurring the mentioned outcome, the following condition should be satisfied, otherwise, non-convergent results with zero answer for {u}, or nonzero answer and locking will be produced.

$$n_u \geq n_\sigma \tag{19}$$

Where $n_u$ and $n_\sigma$ are the number of DOF in the vector {u} of nodal displacements and the number of DOF in the vector {σ} of nodal stresses, respectively. From solvability point of view, the adequate condition requires that the number of zero eigenvalues of the element stiffness matrix is equal to the number of rigid body modes (which is six in the case of solid elements), as shown by Olson [91].

Excluding stability considerations, present element has standard features [88], thus only the basic steps has been reported in this section. Three elastic displacement $U_1$, $U_2$, $U_3$ and three interlaminar stress components are defined as nodal degrees of freedom. Hence, following serendipity [92], linear polynomials are chosen as interpolation functions for every DOF.

$$\mu = \{N\}\{\mu^e\} \tag{20}$$

Where μ and $\mu^e$ represent the displacements and stresses components inside the element and corresponding nodal values, respectively, while {N}= {$N^1$, $N^2$, $N^3$, $N^4$, $N^5$, $N^6$, $N^7$, $N^1$, $N^8$} that is denoted in Appendix B. In order to uniform the computation of the integrals involved in the generation of the element stiffness matrix, commonly, a topological transformation from the physical volume $(x1, x2, x3)^e$ to the natural volume $(\xi_1, \xi_2, \xi_3)^e$ is accomplished, at which the $\xi_j$ is the local, non-dimensional nodal coordinates with origin at the center of the element. To this purpose, the physical coordinates $x_i$ of any point inside the volume of the element are expressed in terms of nodal coordinates $x_j^e$ and interpolation functions N.

$$x_i = \{N\}\{x_i^e\} \quad (i=1,3) \tag{21}$$

This transformation maps any element into a cube with corners at ($\xi_j$= ±1). Then, the derivatives with respect to physical coordinates $x_j$ appearing in the energy integrals are performed in terms of the transformed coordinates $\xi_j$.

Consequently, the stress vector is determined as:

$$\{\sigma\} = [S]\{q_e\} \tag{22}$$

Where $\{\sigma\}^T$= {$\sigma_{11}$, $\sigma_{12}$, $\sigma_{22}$, $\sigma_{13}$, $\sigma_{23}$, $\sigma_{33}$}, and [S] is stiffness matrix.

## 4. Result and Discussion

Due to intrinsically nonlinear behavior of cohesive zone modeling, the nonlinear finite element analysis utilizing full Newton- Raphson iterative method is fulfilled in order to acquire longitudinal modulus ($E_z$), transverse modulus ($E_x$= $E_y$) and interfacial shear and radial stresses of CNT–CF hybrid composite. The finite element result under axial loading is described in Fig. 10.

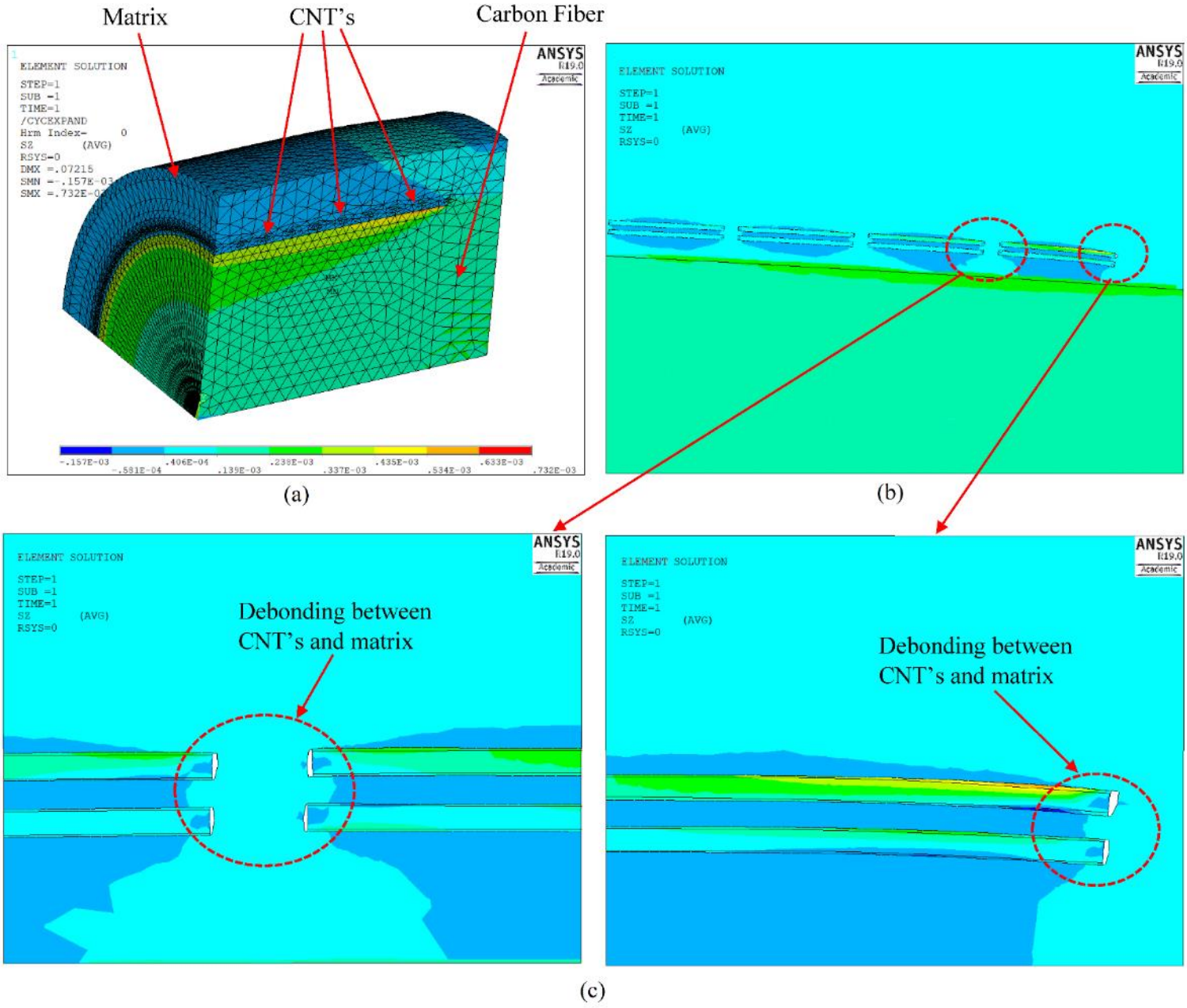


**Fig. 10:** Stress contour of the hybrid composite (a) quarter of the RVE model (b) cut view at micro-interphase region (c) partial view, debonding damage between CNT's and matrix

The uniform displacement is applied to the end of the model and the reaction forces are read from the constrained side of the model, which has been restrained from any movement except radial direction. The longitudinal modulus is expressed as below:

$$E_z = \frac{\sigma_{zz}}{\varepsilon_{zz}} = \frac{L}{\Delta L}\sigma_{ave} \quad ; \ \sigma_{ave} = \frac{F_c}{A} \tag{23}$$

Where L, $F_c$ and A are model length, reaction force at the restricted side and model cross section area, respectively. The mesh convergence study has been conducted in terms of maximum interfacial shear stress utilizing refined mesh which is depicted in the Fig. 11, in which D=1 denotes 21000 elements.

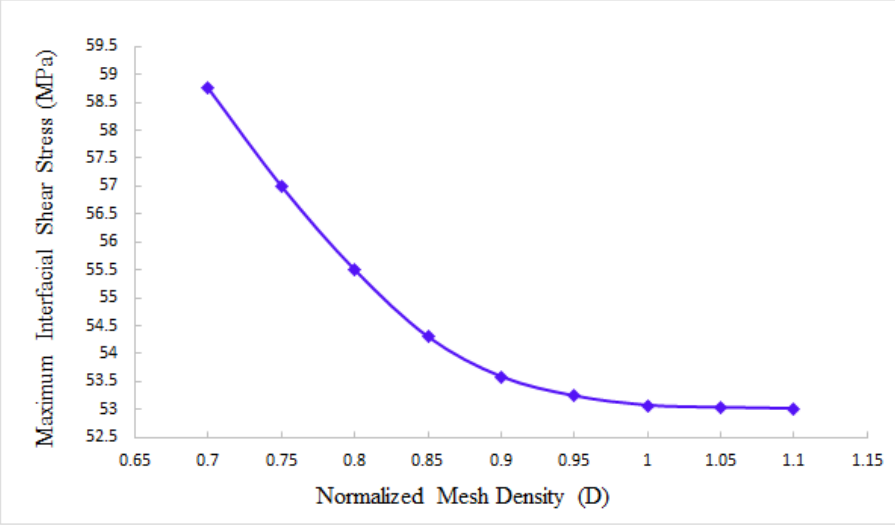


**Fig. 11. N**ormalized mesh density versus maximum interfacial shear stress

The transverse and longitudinal moduli of hybrid composite model containing randomly oriented CNT's versus CNT volume fraction are described in Fig. 12. From the graph supplied, it can be inferred that the carbon nanotubes enhance the transverse elastic modulus of CF–CNT hybrid composite pronouncedly which is about 10 % percent improvement with solely 1% volume fraction, however, the influence on the longitude elastic modulus is negligible. Therefore, employing the CNT's as reinforcement agent for augmenting the longitudinal elastic modulus in the hybrid composites is an unprofitable method. The elastic modulus results manifest excellent agreement with experimental investigations [93] and also user-defined finite element formulation. It should be notified that the effect of debonding between CNT and surrounding matrix on the transverse Young's modulus is about 0.5% at 1% volume fraction (which will enhance by increasing the CNT volume fraction), whereas it doesn't show any alteration in the longitudinal young's modulus of the hybrid composite model.

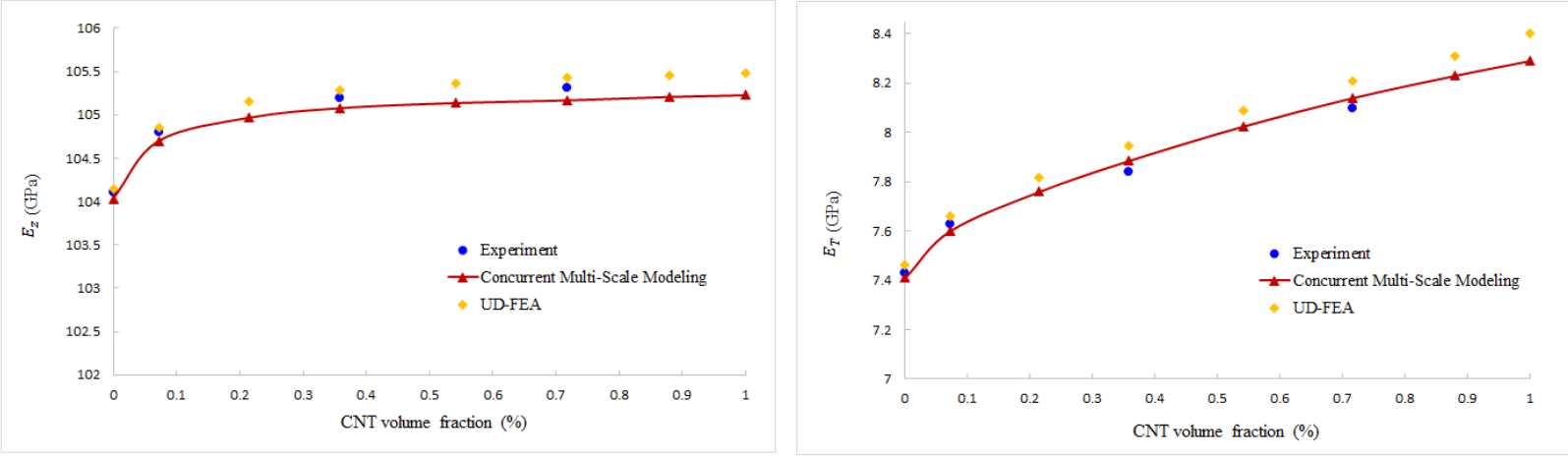


**Fig. 12:** (a) The longitudinal and (b) transverse elastic moduli of CNT–CF reinforced hybrid composite versus CNT volume fraction

Given that the CNT and matrix as 'hollow micro-interphase' region around carbon fiber, an outstanding contribution is made to the carbon fiber–matrix interfacial behavior in the hybrid composite. Therefore, interfacial properties as a fundamental issue in the fiber reinforced composites, is scrutinize in the current work. The distributions of interfacial shear and radial stresses along the carbon fiber length are illustrated in Fig.13. From the graphs provided, it can be inferred that growth of small portion of randomly oriented CNT's on the surface of core fiber (2 wt.%), will strikingly diminishes the interfacial shear and radial stresses by 19.2 % and 21.3%, respectively. As expected, the maximum value of interfacial shear stress occurs in contiguity of the fiber end. Furthermore, rather than the position of maximum stress, the amount of peak shear stress is of critical importance since the debonding between fiber and matrix will ensue if the maximum shear stress exceeds the interfacial shear strength. Employing analytical method, about 21% reduction of the maximum shear stress was achieved by adding small amount of multi-walled carbon nanotubes [93]. With regard to the interfacial radial stress, it is almost zero over 60% of fiber length and rises sharply at the end that can be ascribed to the free-edge effect singularity [94]. Accordingly, maximum magnitude of the radial stress at the ends of the fiber can result in a failure between fiber and matrix which has been mitigated considerably by solely 2 wt.% of CNT's.

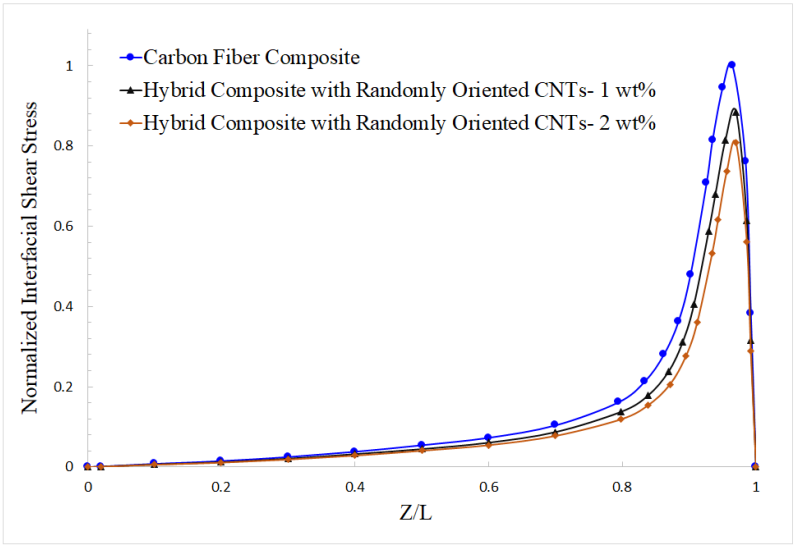


(a)

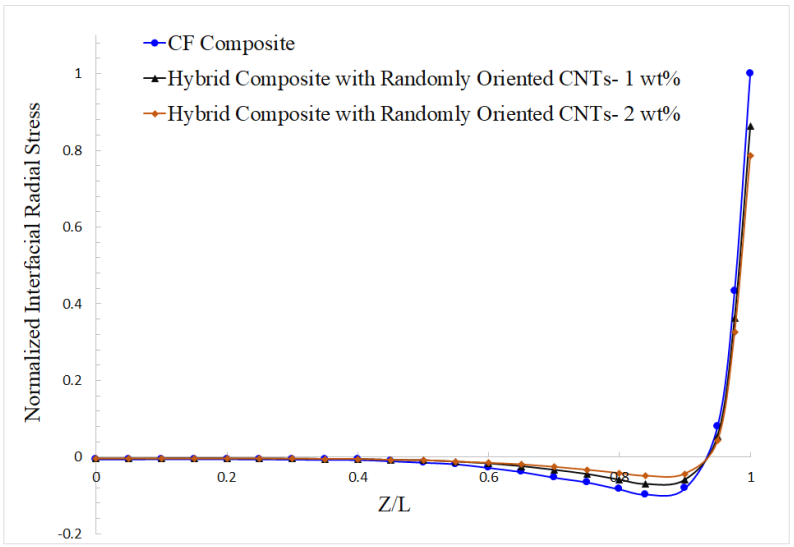


(b)

**Fig. 13:** The normalized interfacial stress distribution, (a) Interfacial shear stress, (b) Interfacial radial stress

It is noteworthy to mention that due to the surface area of core fiber and actual configuration and dispersion of CNT's at matrix, high volume fraction of CNT's doesn't reflect a feasible and practical issue which brings about agglomerated and entangled cluster of CNT's without significant effect on the mechanical properties of resulting multi-scale composite [57,95]. As it can be seen in Fig. 13, increasing the CNT content in the interphase region, diminishes the maximum interfacial stresses, however, it doesn't alter the stress distribution and the positions of maximum stresses. Considering various configurations of carbon nanotubes by 2 wt. %, the interfacial stresses of CF–CNT hybrid composite are delineated in the Fig.14. The results reveal that the configuration of CNT's at micro-interphase region plays a prominent role in the load transferring mechanism and therefore leads to striking difference of interfacial properties. As it is displayed, axially aligned and radially oriented CNT's exhibit the highest and lowest reinforcement impacts on the interfacial properties, respectively, while the hybrid composite with randomly oriented CNT's shows reinforcement magnitude between the two above-mentioned configurations. It is worth of notice that the models with radially oriented CNT's and axially aligned CNT's can be introduced as lower and upper bounds of reinforcement values, in which the latter makes a valuable contributes in reinforcing the interfacial properties under axial loading that can be used as a remarkable issue in designing advanced composite structure. Furthermore, as it

can be seen in Fig.14, the hybrid composite with randomly oriented CNT's represents much improved interfacial properties than those of with radially aligned CNT's. Similarly, and prominently, in accordance with the experimental investigations carried out by Sager et. al [96], randomly oriented and radially aligned MWCNT coated fibers demonstrated a 71% and 11% increase in interfacial shear strength. Consequently, it can be concluded that by aligning the carbon nanotubes at micro-interphase region along the axial direction of core fiber, the maximum interfacial properties can be achieved in unidirectional coated-fibers composites under axial loading.

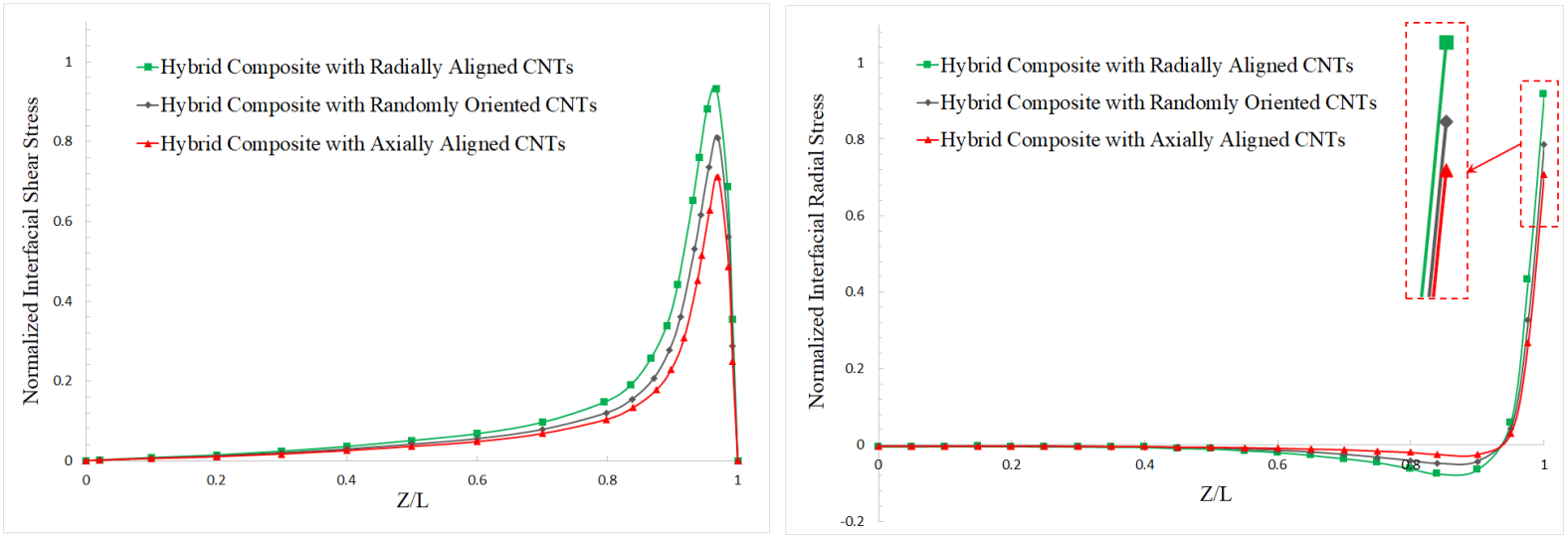


(a) (b)

**Fig. 14:** The normalized interfacial stress distribution for different CNT's configurations, (a) Interfacial shear stress, (b) Interfacial radial stress

Multi-scale composites can be classified into two types of systems entitled as 'hybrid fiber system' and 'mixed CNT/matrix system' illustrated in Fig. 15. As a crucial issue, both foregoing systems are deemed as hybrid multi-scale composites while they reflect dissonant interfacial properties which should be addressed during designing and analysis of such materials. Thus, in order to profound understanding of in situ morphology of nano-materials influences on the multi-scale composites, this section of present work is allocated to the mentioned issue. Characterizing the in-situ properties of multi-scale composite materials, a new experimental technique was presented by Wood et. al [32] that enables local stiffness mapping of a CNT-reinforced matrix in the region

surrounding fibers which provides a powerful tool to engineers who aim to appraise local reinforcement gradients.

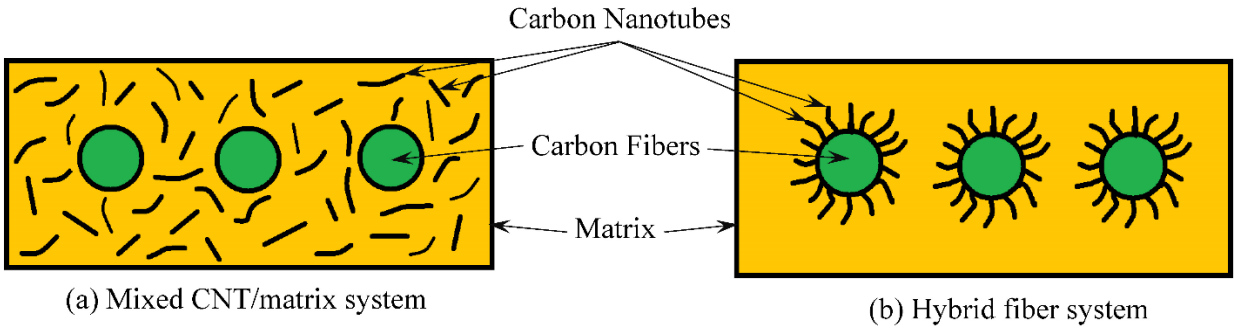


**Fig. 15:** Schematic illustration of two systems of multi-scale hybrid composites; (a) Mixed CNT/ matrix system, (b) Hybrid fiber system

Considering two aforementioned systems, the distribution of interfacial shear and radial stresses are represented in Fig.16. As it can be seen, exerting 'mixed CNT/ matrix system' will pronouncedly decline the influence of nano-reinforcement phase on the interfacial properties of such materials. Moreover, the maximum interfacial shear and radial stresses of 'mixed CNT/ matrix system' decrease solely 5.3 % and 6.6 %, respectively, than CF–composite which is a vital outcome in designing multi-scale hybrid composites. As a consequence, the presence of 'mixed CNT/ Matrix system' doesn't make contribution to the interfacial behavior with respect to 'hybrid fiber system', which should be addressed in analysis and manufacturing of CNT–CF hybrid composites under different loading.

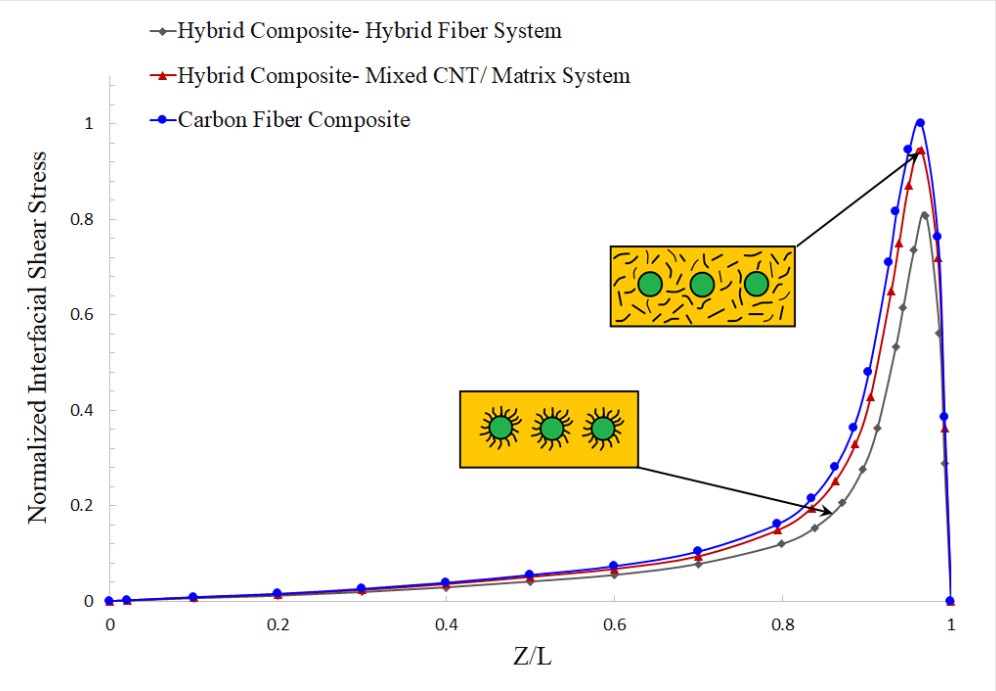


(a)

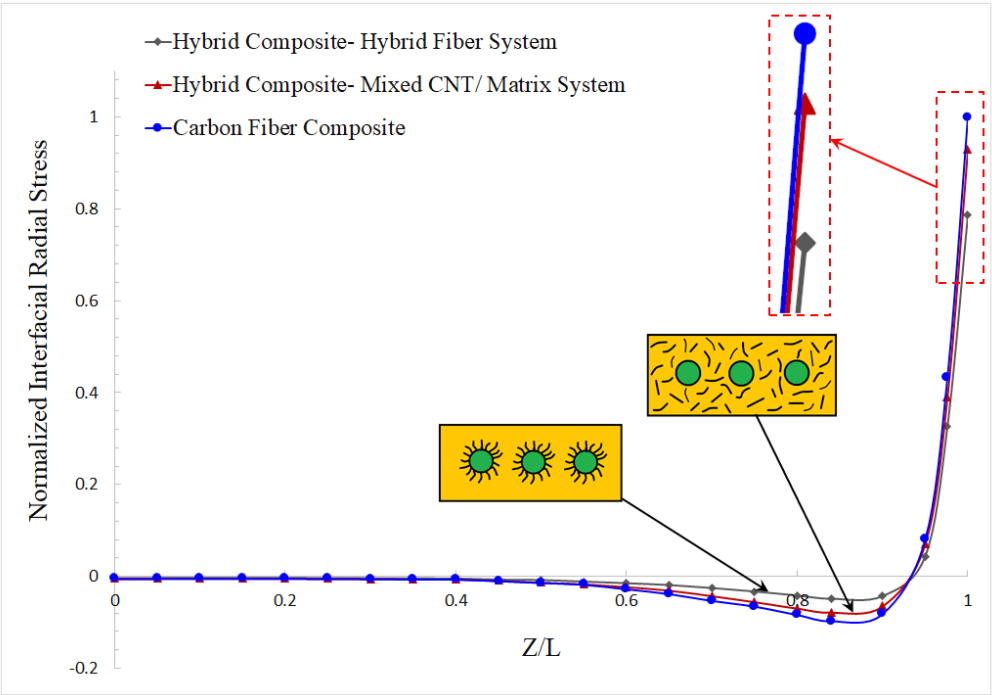


(b)

**Fig. 16:** The interfacial stress distribution for different hybrid system (a) Interfacial shear stress (b) Interfacial radial stress

Fig. 17 describes a comparison of normalized maximum interfacial shear stress versus CNT content consisting of various CNT's orientations. From the graph supplied, it is evident that by increasing the CNT's quantity in the micro-interphase region, the maximum interfacial shear stress declines extraordinarily. Likewise, the differences between maximum stresses of various CNT's configurations are inconsequential at low weight percentage whereas it exhibits notable disparity at higher amount of CNT's. Adding only 2 wt.% of carbon nanotubes, engenders to diminish the maximum interfacial shear stress by 19.2 % and 28.9%, considering randomly and axially aligned CNT's, respectively.

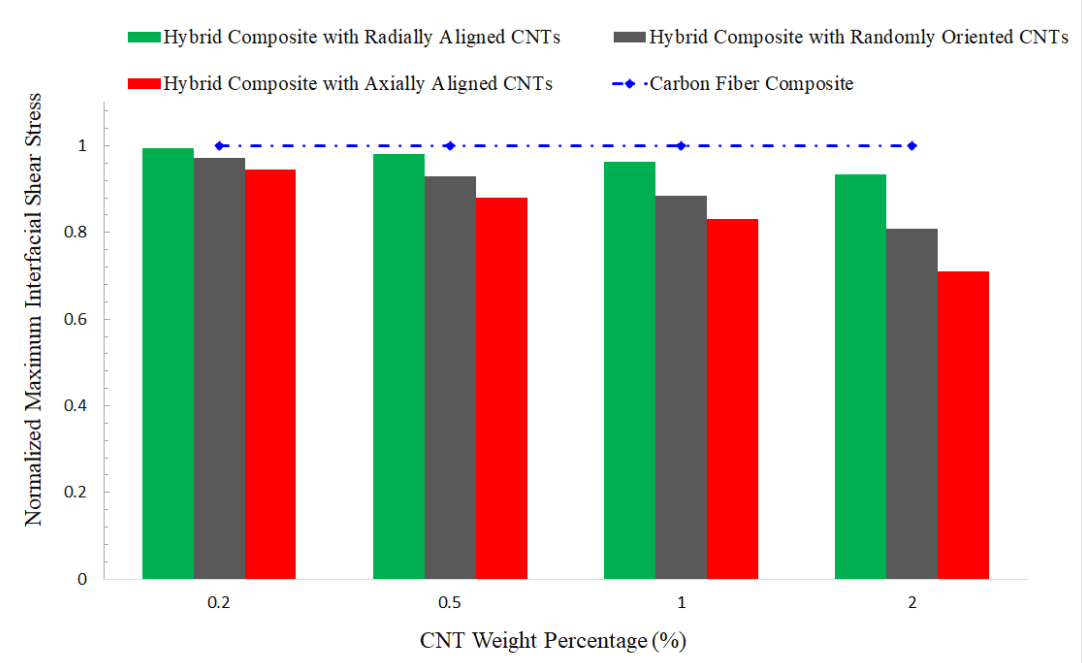


**Fig. 17:** The normalized maximum interfacial shear stress versus CNT weight percentage

As a momentous issue, load transferring phenomenon plays a crucial role in defining the mechanical properties of CNT–CF hybrid composites. It should be mentioned that imperfect bonding between the grown CNT's and encircling matrix at nanoscale, affects the micro-interphase mechanic behavior [71] and therefore impresses the load transfer phenomenon between fibers and matrix at macro-scale. Hence, in order to construct much accurate region around the core fiber, non-bonded interphase via vdW interactions has been taken into account between CNT's and matrix as stated in section 2.2. The effect of non-bonded interphase on the maximum interfacial shear and radial stresses in terms of without CZM to with CZM ratio, can be seen in Fig.18 and

Fig.19, respectively, considering different orientations of carbon nanotubes in the micro-interphase region. A glance at the two figures provided discloses remarkable influence of non-bonded interphase region on the interfacial properties specially at higher volume fractions, indicating almost similar trends for both interfacial shear and radial stresses. Moreover, it can be understood that the influence of non-bonded interphase between CNT and matrix is more significant in axially and randomly orientations than radially grown configuration. Hence, considering mere 2 wt% of CNT's, the imperfect bonding represents a pronounced discrepancy of interfacial shear stress with respect to perfect bonding, regarding axially aligned and randomly oriented configurations, as 6.2 % and 5.11%, respectively. Analogously, considering non-bonded interphase and perfect bonding, notable reduction of interfacial radial stress is manifested regarding axially aligned and random oriented CNT's as 6.42 % and 5.25%, respectively. In contrast to elastic moduli, therefore, taking into account the non-bonded interphase region between CNT's and matrix precludes overestimating the outcomes and plays a momentous role on interfacial properties of multi-scale hybrid composites.

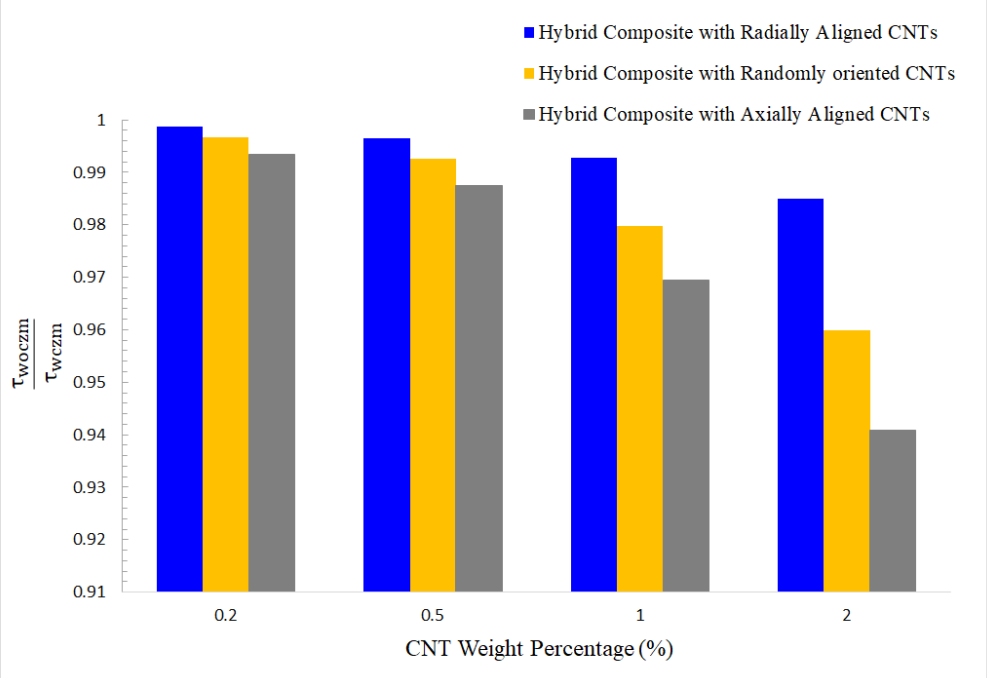


**Fig. 18:** The maximum interfacial shear stress ratio considering perfect bond and debonding condition

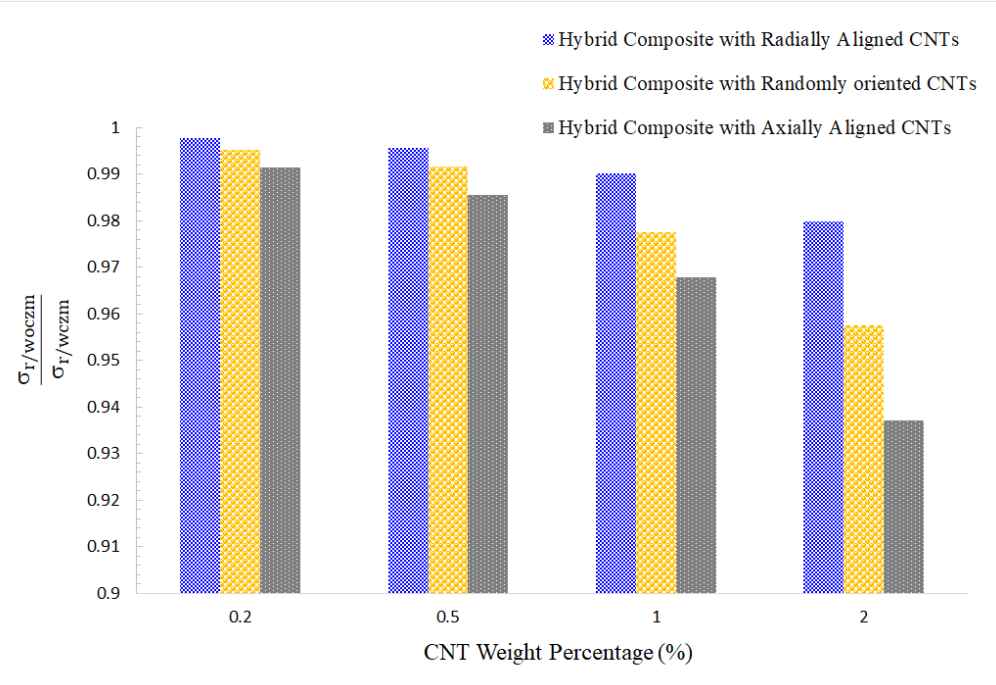


**Fig. 19:** The maximum interfacial radial stress ratio considering perfect bond and debonding condition

Analogous to interfacial shear stress, in spite of small portion of CNT's in the micro-interphase region, the interfacial radial stress dwindles which yields higher interfacial strength and precluding debonding between fiber and matrix in the unidirectional composite materials. As shown in Fig. 20, a prominent reduction is gained with only 2 wt.% of CNT's by 21.3 %, considering randomly oriented carbon nanotubes.

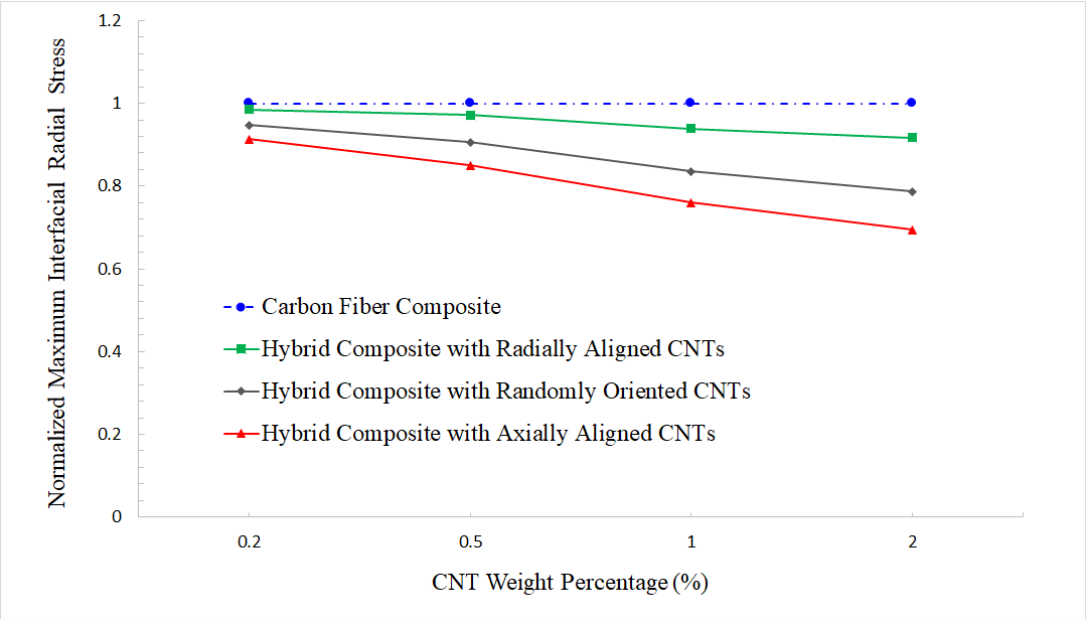


**Fig. 20:** The normalized maximum interfacial radial stress versus CNT weight percentage

## 5. Conclusion

Present work is devoted to mechanical properties of unidirectional carbon nanotube–carbon fiber reinforced hybrid composites utilizing 3D finite element multi-scale modeling. The constructed multi-scale model consists of carbon nanotubes (CNT's), carbon fiber (CF), non-bonded interphase region and surrounding matrix, covering all incorporated scales of nano, micro, meso and macro. The non-bonded interphase region between CNT's and matrix is established employing cohesive zone model (CZM). The interfacial behavior is assessed considering three different configurations of grown CNT's on the fiber surface, encompassing radially, axially and randomly oriented CNT's. The outcomes divulge a considerable reduction of fiber-matrix interfacial shear stresses in the hybrid composite containing axially and randomly oriented CNT's by 28.9% and 19.2 %, respectively, with solely 2 wt.% of CNT's. Investigating two hybrid systems, it is remarkably disclosed that composites with CNT's–coated fibers represent much proper interfacial behaviors than those with CNT reinforcements in matrix. Considering non-bonded interphase region between CNT's and surrounding matrix, the results manifest pronounced effect on the interfacial properties, whereas no influence on the Young's moduli is observed, especially at lower volume fractions. Finally, the results demonstrate that the presence of CNT's improves the

transverse Young's modulus, however, it shows negligible effect on the longitudinal Young's modulus.

## Appendix A

The Eshelby tensor elements [$S_r$] for cylindrical reinforcement[97]:

$$S_{1111} = 0, \qquad S_{2222} = S_{3333} = \frac{5-4\upsilon_m}{8(1-\upsilon_m)},$$

$$S_{2233} = S_{3322} = \frac{4\upsilon_m - 1}{8(1-\upsilon_m)},$$

$$S_{1122} = S_{1133} = 0, \qquad S_{2211} = S_{3311} = \frac{\upsilon_m}{2(1-\upsilon_m)},$$

$$S_{1212} = S_{1313} = \frac{1}{4}, \qquad S_{2323} = \frac{3-4\upsilon_m}{8(1-\upsilon_m)},$$

Where $\upsilon_m$ is Poisson's ratio of matrix.

## Appendix B

Serendipity linear polynomials are represented as:

$$N^1 = 0.125(1-\zeta_1)(1-\zeta_2)(1-\zeta_3)$$

$$N^2 = 0.125(1+\zeta_1)(1-\zeta_2)(1-\zeta_3)$$

$$N^3 = 0.125(1+\zeta_1)(1+\zeta_2)(1-\zeta_3)$$

$$N^4 = 0.125(1-\zeta_1)(1+\zeta_2)(1-\zeta_3)$$

$$N^5 = 0.125(1-\zeta_1)(1-\zeta_2)(1+\zeta_3)$$

$$N^6 = 0.125(1+\zeta_1)(1-\zeta_2)(1+\zeta_3)$$

$$N^7 = 0.125(1+\zeta_1)(1+\zeta_2)(1+\zeta_3)$$

$$N^8 = 0.125(1-\zeta_1)(1+\zeta_2)(1+\zeta_3)$$

## References


[1] Miller B, Muri P, Rebenfeld L. A microbond method for determination of the shear strength of a fiber/resin interface. Compos Sci Technol 1987;28:17–32. doi:https://doi.org/10.1016/0266-3538(87)90059-5.

[2] Icardi U, Sciuva M Di, Librescu L. Dynamic response of adaptive cross-ply cantilevers featuring interlaminar bonding imperfections. AIAA J 2000;38:499–506.

[3] Icardi U, Sola F. Recovering critical stresses in sandwiches using through-the-thickness reinforcement. Compos Part B Eng 2013;54:269–77.

[4] Icardi U, Sola F. Analysis of bonded joints with laminated adherends by a variable kinematics layerwise model. Int J Adhes Adhes 2014;50:244–54.

[5] Kim J-K, Mai Y-W. Engineered interfaces in fiber reinforced composites. Elsevier; 1998.

[6] Ramdoum S, Fekirini H, Bouafia F, Benbarek S, Serier B, Feo L. Carbone/epoxy interface debond growth using the Contour Integral/Cohesive zone method. Compos Part B Eng 2018;142:102–7. doi:10.1016/J.COMPOSITESB.2018.01.011.

[7] Drzal LT, Rich MJ, Lloyd PF. Adhesion of graphite fibers to epoxy matrices: I. The role of fiber surface treatment. J Adhes 1983;16:1–30.

[8] Green KJ, Dean DR, Vaidya UK, Nyairo E. Multiscale fiber reinforced composites based on a carbon nanofiber/epoxy nanophased polymer matrix: Synthesis, mechanical, and thermomechanical behavior. Compos Part A Appl Sci Manuf 2009. doi:10.1016/j.compositesa.2009.05.010.

[9] Agarwal BD, Bansal RK. Effect of an interfacial layer on the properties of fibrous composites: a theoretical analysis. Fibre Sci Technol 1979;12:149–58.

[10] Jain R, Vaidya UK, Haque A. Processing and characterization of carbon-carbon nanofiber composites. Adv Compos Mater 2006;15:211–41. doi:10.1163/156855106777873905.

[11] Ho M, Wang H, Lau K, Lee J. Interfacial bonding and degumming effects on silk

fibre/polymer biocomposites. Compos Part B Eng 2012;43:2801–12. doi:10.1016/J.COMPOSITESB.2012.04.042.

[12] Thomsen OT, Charca S. Assessment of the Interface Shear Strength of Metal-Polymer System Based on the Single Filament Fragmentation Test Method. Appl Mech Mater 2011;70:446–51. doi:10.4028/www.scientific.net/AMM.70.446.

[13] Ascione L, Berardi VP, Feo L, Mancusi G. A numerical evaluation of the interlaminar stress state in externally FRP plated RC beams. Compos Part B Eng 2005;36:83–90. doi:10.1016/S1359-8368(03)00018-0.

[14] Icardi U, Ferrero L. Optimisation of sandwich panels with functionally graded core and faces. Compos Sci Technol 2009;69:575–85. doi:10.1016/J.COMPSCITECH.2008.11.036.

[15] Ghasemi H, Kerfriden P, Bordas SPA, Muthu J, Zi G, Rabczuk T. Interfacial shear stress optimization in sandwich beams with polymeric core using non-uniform distribution of reinforcing ingredients. Compos Struct 2015;120:221–30. doi:10.1016/J.COMPSTRUCT.2014.10.005.

[16] Rafiee R, Moghadam RM. On the modeling of carbon nanotubes: a critical review. Compos Part B Eng 2014;56:435–49.

[17] Hosseini SA, Saber-Samandari S, Maleki Moghadam R. Multiscale modeling of interface debonding effect on mechanical properties of nanocomposites. Polym Compos 2017;38:789–96.

[18] Zahedi M, Malekimoghadam R, Rafiee R, Icardi U. A study on fracture behavior of semi-elliptical 3D crack in clay-polymer nanocomposites considering interfacial debonding. Eng Fract Mech 2019;209:245–59.

[19] Moghadam RM, Saber-Samandari S, Hosseini SA. On the tensile behavior of clay–epoxy nanocomposite considering interphase debonding damage via mixed-mode cohesive zone material. Compos Part B Eng 2016;89:303–15.

[20] Vu-Bac N, Silani M, Lahmer T, Zhuang X, Rabczuk T. A unified framework for stochastic predictions of mechanical properties of polymeric nanocomposites. Comput

Mater Sci 2015. doi:10.1016/j.commatsci.2014.04.066.

[21] Vu-Bac N, Lahmer T, Zhang Y, Zhuang X, Rabczuk T. Stochastic predictions of interfacial characteristic of polymeric nanocomposites (PNCs). Compos Part B Eng 2014. doi:10.1016/j.compositesb.2013.11.014.

[22] Hamdia KM, Silani M, Zhuang X, He P, Rabczuk T. Stochastic analysis of the fracture toughness of polymeric nanoparticle composites using polynomial chaos expansions. Int J Fract 2017;206:215–27. doi:10.1007/s10704-017-0210-6.

[23] Msekh MA, Cuong NH, Zi G, Areias P, Zhuang X, Rabczuk T. Fracture properties prediction of clay/epoxy nanocomposites with interphase zones using a phase field model. Eng Fract Mech 2018;188:287–99. doi:10.1016/J.ENGFRACMECH.2017.08.002.

[24] Zhang Y, Zhuang X, Muthu J, Mabrouki T, Fontaine M, Gong Y, et al. Load transfer of graphene/carbon nanotube/polyethylene hybrid nanocomposite by molecular dynamics simulation. Compos Part B Eng 2014. doi:10.1016/j.compositesb.2014.03.009.

[25] Odegard GM, Gates TS, Wise KE, Park C, Siochi EJ. Constitutive modeling of nanotube-reinforced polymer composites. Compos Sci Technol 2003. doi:10.1016/S0266-3538(03)00063-0.

[26] Mousavi AA, Arash B, Zhuang X, Rabczuk T. A coarse-grained model for the elastic properties of cross linked short carbon nanotube/polymer composites. Compos Part B Eng 2016;95:404–11.

[27] Silvestre N, Faria B, Canongia Lopes JN. Compressive behavior of CNT-reinforced aluminum composites using molecular dynamics. Compos Sci Technol 2014. doi:10.1016/j.compscitech.2013.09.027.

[28] Qian D, Dickey EC, Andrews R, Rantell T. Load transfer and deformation mechanisms in carbon nanotube-polystyrene composites. Appl Phys Lett 2000;76:2868–70.

[29] Schadler LS, Giannaris SC and, Ajayan PM. Load transfer in carbon nanotube epoxy composites. Appl Phys Lett 1998;73:3842–4.

[30] Rodriguez AJ, Guzman ME, Lim C-S, Minaie B. Mechanical properties of carbon

nanofiber/fiber-reinforced hierarchical polymer composites manufactured with multiscale-reinforcement fabrics. Carbon N Y 2011;49:937–48.

[31] Thostenson ET, Li WZ, Wang DZ, Ren ZF, Chou TW. Carbon nanotube/carbon fiber hybrid multiscale composites. J Appl Phys 2002;91:6034–7. doi:10.1063/1.1466880.

[32] Wood CD, Palmeri MJ, Putz KW, Ho G, Barto R, Brinson LC. Nanoscale structure and local mechanical properties of fiber-reinforced composites containing MWCNT-grafted hybrid glass fibers. Compos Sci Technol 2012;72:1705–10.

[33] Yao X, Gao X, Jiang J, Xu C, Deng C, Wang J. Comparison of carbon nanotubes and graphene oxide coated carbon fiber for improving the interfacial properties of carbon fiber/epoxy composites. Compos Part B Eng 2018;132:170–7. doi:https://doi.org/10.1016/j.compositesb.2017.09.012.

[34] Rafiee R, Ghorbanhosseini A. Predicting mechanical properties of fuzzy fiber reinforced composites: radially grown carbon nanotubes on the carbon fiber. Int J Mech Mater Des 2018;14:37–50. doi:10.1007/s10999-016-9359-9.

[35] Lachman N, Wiesel E, Guzman de Villoria R, Wardle BL, Wagner HD. Interfacial load transfer in carbon nanotube/ceramic microfiber hybrid polymer composites. Compos Sci Technol 2012;72:1416–22. doi:https://doi.org/10.1016/j.compscitech.2012.05.015.

[36] Sebastian J, Schehl N, Bouchard M, Boehle M, Li L, Lagounov A, et al. Health monitoring of structural composites with embedded carbon nanotube coated glass fiber sensors. Carbon N Y 2014;66:191–200. doi:https://doi.org/10.1016/j.carbon.2013.08.058.

[37] Zhou HW, Mishnaevsky L, Yi HY, Liu YQ, Hu X, Warrier A, et al. Carbon fiber/carbon nanotube reinforced hierarchical composites: Effect of CNT distribution on shearing strength. Compos Part B Eng 2016;88:201–11. doi:10.1016/J.COMPOSITESB.2015.10.035.

[38] Lee M-W, Wang T-Y, Tsai J-L. Characterizing the interfacial shear strength of graphite/epoxy composites containing functionalized graphene. Compos Part B Eng 2016;98:308–13. doi:https://doi.org/10.1016/j.compositesb.2016.05.001.

[39] Zhang X, Fan X, Yan C, Li H, Zhu Y, Li X, et al. Interfacial Microstructure and

Properties of Carbon Fiber Composites Modified with Graphene Oxide. ACS Appl Mater Interfaces 2012;4:1543–52. doi:10.1021/am201757v.

[40] Aziz S, Rashid SA, Rahmanian S, Salleh MA. Experimental evaluation of the interfacial properties of carbon nanotube coated carbon fiber reinforced hybrid composites. Polym Compos 2015;36:1941–50. doi:10.1002/pc.23103.

[41] Garcia EJ, Wardle BL, John Hart A. Joining prepreg composite interfaces with aligned carbon nanotubes. Compos Part A Appl Sci Manuf 2008;39:1065–70. doi:https://doi.org/10.1016/j.compositesa.2008.03.011.

[42] Garcia EJ, Wardle BL, John Hart A, Yamamoto N. Fabrication and multifunctional properties of a hybrid laminate with aligned carbon nanotubes grown In Situ. Compos Sci Technol 2008;68:2034–41. doi:https://doi.org/10.1016/j.compscitech.2008.02.028.

[43] Radue MS, Odegard GM. Multiscale modeling of carbon fiber/carbon nanotube/epoxy hybrid composites: Comparison of epoxy matrices. Compos Sci Technol 2018;166:20–6.

[44] Ma X, Scarpa F, Peng H-X, Allegri G, Yuan J, Ciobanu R. Design of a hybrid carbon fibre/carbon nanotube composite for enhanced lightning strike resistance. Aerosp Sci Technol 2015;47:367–77.

[45] Pal G, Kumar S. Multiscale modeling of effective electrical conductivity of short carbon fiber-carbon nanotube-polymer matrix hybrid composites. Mater Des 2016;89:129–36.

[46] Chatzigeorgiou G, Seidel GD, Lagoudas DC. Effective mechanical properties of “fuzzy fiber” composites. Compos Part B Eng 2012;43:2577–93.

[47] Dai G, Mishnaevsky Jr L. Carbon nanotube reinforced hybrid composites: Computational modeling of environmental fatigue and usability for wind blades. Compos Part B Eng 2015;78:349–60.

[48] Kulkarni M, Carnahan D, Kulkarni K, Qian D, Abot JL. Elastic response of a carbon nanotube fiber reinforced polymeric composite: a numerical and experimental study. Compos Part B Eng 2010;41:414–21.

[49] Kundalwal SI, Kumar S. Multiscale modeling of stress transfer in continuous microscale

fiber reinforced composites with nano-engineered interphase. Mech Mater 2016;102:117–31.

[50] Kundalwal SI, Ray MC. Effect of carbon nanotube waviness on the effective thermoelastic properties of a novel continuous fuzzy fiber reinforced composite. Compos Part B Eng 2014;57:199–209. doi:10.1016/J.COMPOSITESB.2013.10.003.

[51] Kundalwal SI, Meguid SA. Multiscale modeling of regularly staggered carbon fibers embedded in nano-reinforced composites. Eur J Mech 2017;64:69–84.

[52] Kundalwal SI, Ray MC. Micromechanical analysis of fuzzy fiber reinforced composites. Int J Mech Mater Des 2011;7:149–66. doi:10.1007/s10999-011-9156-4.

[53] Kundalwal SI, Ray MC. Effective properties of a novel composite reinforced with short carbon fibers and radially aligned carbon nanotubes. Mech Mater 2012;53:47–60. doi:10.1016/J.MECHMAT.2012.05.008.

[54] Kundalwal SI, Ray MC. Effective properties of a novel continuous fuzzy-fiber reinforced composite using the method of cells and the finite element method. Eur J Mech - A/Solids 2012;36:191–203. doi:10.1016/J.EUROMECHSOL.2012.03.006.

[55] Ren X, Burton J, Seidel GD, Lafdi K. Computational multiscale modeling and characterization of piezoresistivity in fuzzy fiber reinforced polymer composites. Int J Solids Struct 2015;54:121–34.

[56] Bekyarova E, Thostenson ET, Yu A, Kim H, Gao J, Tang J, et al. Multiscale carbon nanotube− carbon fiber reinforcement for advanced epoxy composites. Langmuir 2007;23:3970–4.

[57] Yamamoto N, Hart AJ, Garcia EJ, Wicks SS, Duong HM, Slocum AH, et al. High-yield growth and morphology control of aligned carbon nanotubes on ceramic fibers for multifunctional enhancement of structural composites. Carbon N Y 2009;47:551–60.

[58] Zhao Z-G, Ci L-J, Cheng H-M, Bai J-B. The growth of multi-walled carbon nanotubes with different morphologies on carbon fibers. Carbon N Y 2005;43:663–5.

[59] Talebi H, Silani M, Bordas SPA, Kerfriden P, Rabczuk T. A computational library for

multiscale modeling of material failure. Comput Mech 2014;53:1047–71. doi:10.1007/s00466-013-0948-2.

[60] Budarapu PR, Gracie R, Yang S-W, Zhuang X, Rabczuk T. Efficient coarse graining in multiscale modeling of fracture. Theor Appl Fract Mech 2014;69:126–43. doi:10.1016/J.TAFMEC.2013.12.004.

[61] Kalamkarov AL, Georgiades A V, Rokkam SK, Veedu VP, Ghasemi-Nejhad MN. Analytical and numerical techniques to predict carbon nanotubes properties. Int J Solids Struct 2006;43:6832–54.

[62] Li C, Chou T-W. A structural mechanics approach for the analysis of carbon nanotubes. Int J Solids Struct 2003;40:2487–99.

[63] Yakobson BI, Brabec CJ, Bernholc J. Structural mechanics of carbon nanotubes: from continuum elasticity to atomistic fracture. J Comput Mater Des 1996;3:173–82.

[64] Silvestre N. On the accuracy of shell models for torsional buckling of carbon nanotubes. Eur J Mech A/Solids 2012. doi:10.1016/j.euromechsol.2011.09.005.

[65] Bagchi A, Nomura S. On the effective thermal conductivity of carbon nanotube reinforced polymer composites. Compos Sci Technol 2006;66:1703–12. doi:https://doi.org/10.1016/j.compscitech.2005.11.003.

[66] Choi M, Eom K, Gwak K, Dai MD, Olshevskiy A, Kim C-W. Dynamical response of multi-walled carbon nanotube resonators based on continuum mechanics modeling for mass sensing applications. J Mech Sci Technol 2017;31:2385–91. doi:10.1007/s12206-017-0435-3.

[67] Yao N, Lordi V. Young's modulus of single-walled carbon nanotubes. J Appl Phys 1998;84:1939–43.

[68] Salvetat J-P, Briggs GAD, Bonard J-M, Bacsa RR, Kulik AJ, Stöckli T, et al. Elastic and shear moduli of single-walled carbon nanotube ropes. Phys Rev Lett 1999;82:944.

[69] Palaci I, Fedrigo S, Brune H, Klinke C, Chen M, Riedo E. Radial elasticity of multiwalled carbon nanotubes. Phys Rev Lett 2005;94:175502.

[70] Sinnott SB. Chemical functionalization of carbon nanotubes. J Nanosci Nanotechnol 2002;2:113–23.

[71] Li C, Chou T-W. Multiscale modeling of compressive behavior of carbon nanotube/polymer composites. Compos Sci Technol 2006;66:2409–14.

[72] Tserpes KI, Chanteli A. Parametric numerical evaluation of the effective elastic properties of carbon nanotube-reinforced polymers. Compos Struct 2013. doi:10.1016/j.compstruct.2012.12.004.

[73] Battezzati L, Pisani C, Ricca F. Equilibrium conformation and surface motion of hydrocarbon molecules physisorbed on graphit. J Chem Soc Faraday Trans 2 Mol Chem Phys 1975;71:1629–39.

[74] Rafiee R, Moghadam RM. Simulation of impact and post-impact behavior of carbon nanotube reinforced polymer using multi-scale finite element modeling. Comput Mater Sci 2012;63:261–8.

[75] Jiang LY, Huang Y, Jiang H, Ravichandran G, Gao H, Hwang KC, et al. A cohesive law for carbon nanotube/polymer interfaces based on the van der Waals force. J Mech Phys Solids 2006;54:2436–52.

[76] Tan H, Jiang LY, Huang Y, Liu B, Hwang KC. The effect of van der Waals-based interface cohesive law on carbon nanotube-reinforced composite materials. Compos Sci Technol 2007;67:2941–6.

[77] Gou J, Minaie B, Wang B, Liang Z, Zhang C. Computational and experimental study of interfacial bonding of single-walled nanotube reinforced composites. Comput Mater Sci 2004;31:225–36.

[78] Volokh KY. Comparison between cohesive zone models. Commun Numer Methods Eng 2004;20:845–56.

[79] ANSYS. ANSYS Mechanical APDL Theory Reference. ANSYS Inc 2016. doi:www.ansys.com.

[80] Foulk JW, Allen DH, Helms KLE. Formulation of a three-dimensional cohesive zone

model for application to a finite element algorithm. Comput Methods Appl Mech Eng 2000;183:51–66. doi:https://doi.org/10.1016/S0045-7825(99)00211-X.

[81] Honjo K. Thermal stresses and effective properties calculated for fiber composites using actual cylindrically-anisotropic properties of interfacial carbon coating. Carbon N Y 2007;45:865–72.

[82] Miyagawa H, Mase T, Sato C, Drown E, Drzal LT, Ikegami K. Comparison of experimental and theoretical transverse elastic modulus of carbon fibers. Carbon N Y 2006;44:2002–8.

[83] Mori T, Tanaka K. Average stress in matrix and average elastic energy of materials with misfitting inclusions. Acta Metall 1973. doi:10.1016/0001-6160(73)90064-3.

[84] Wang J, Pyrz R. Prediction of the overall moduli of layered silicate-reinforced nanocomposites-part I: Basic theory and formulas. Compos Sci Technol 2004. doi:10.1016/S0266-3538(03)00024-1.

[85] Lu P, Leong YW, Pallathadka PK, He CB. Effective moduli of nanoparticle reinforced composites considering interphase effect by extended double-inclusion model–Theory and explicit expressions. Int J Eng Sci 2013;73:33–55.

[86] Chen T, Dvorak GJ, Benveniste Y. Mori-Tanaka estimates of the overall elastic moduli of certain composite materials. J Appl Mech 1992;59:539–46.

[87] Mura T. Micromechanics of defects in solids. Springer Science & Business Media; 2013.

[88] Icardi U, Atzori A. Simple, efficient mixed solid element for accurate analysis of local effects in laminated and sandwich composites. Adv Eng Softw 2004;35:843–59.

[89] Reissner E. On a variational theorem in elasticity. J Math Phys 1950;29:90–5.

[90] Babuška I. The finite element method with Lagrangian multipliers. Numer Math 1973;20:179–92. doi:10.1007/BF01436561.

[91] Olson MD. The mixed finite element method in elasticity and elastic contact problems. Int. Symp. Hybrid Mix. Finite Elem. Methods, Atlanta, GA, 1981, p. 1981.

[92] Zienkiewicz OC, Taylor RL, Zhu JZ. The finite element method: its basis and

fundamentals. Elsevier; 2005.

[93] Shokrieh MM, Daneshvar A, Akbari S. Reduction of thermal residual stresses of laminated polymer composites by addition of carbon nanotubes. Mater Des 2014;53:209–16.

[94] Lessard LB, Schmidt AS, Shokrieh MM. Three-dimensional stress analysis of free-edge effects in a simple composite cross-ply laminate. Int J Solids Struct 1996;33:2243–59.

[95] Chanteli A, Tserpes KI. Finite element modeling of carbon nanotube agglomerates in polymers. Compos Struct 2015;132:1141–8.

[96] Sager RJ, Klein PJ, Lagoudas DC, Zhang Q, Liu J, Dai L, et al. Effect of carbon nanotubes on the interfacial shear strength of T650 carbon fiber in an epoxy matrix. Compos Sci Technol 2009;69:898–904.

[97] Qiu YP, Weng GJ. On the application of Mori-Tanaka's theory involving transversely isotropic spheroidal inclusions. Int J Eng Sci 1990;28:1121–37.